Journal of Petroleum Science and Engineering 210 (2022) 110035

Contents lists available at ScienceDirect

Journal of Petroleum Science and Engineering

journal homepage: www.elsevier.com/locate/petrol

Mechanisms for the anisotropic enrichment of organic matter in saline lake basin: A case study of the Early Eocene Dongpu Depression, eastern China

Fujie Jiang [a,b,*], Di Chen [a,b,**], Chenxi Zhu [a,b], Kangchao Ning [c], Lin Ma [d], Tianwu Xu [e], Ru Qin [a,b], Boshi Li [a,b], Yuanyuan Chen [a,b], Lina Huo [a,b], Zhi Xu [a,b]

[a] State Key Laboratory of Petroleum Resources and Prospecting, China University of Petroleum, Beijing, 102249, China
[b] College of Geosciences, China University of Petroleum, Beijing, 102249, China
[c] Guangdong Bureau of Coal Geology Prospecting Institute, Guangzhou, 510170, China
[d] Henry Moseley X-ray Imaging Facility, University of Manchester, UK
[e] Research Institute of Exploration and Development, Zhongyuan Oilfield Company, SINOPEC, Puyang, 457001, China

ARTICLE INFO

Keywords:
Organic matter enrichment
Saline sediments
Eocene shale sediments
Shale oil exploration
Bohai Bay basin

ABSTRACT

Organic-rich terrestrial shales, the most promising shale oil production layer, are widely distributed in major basins in China, and they are usually interbedded salt rocks. Understanding the role of salt rocks in the organic matter (OM) enrichment in shale sediments has important enlightenment for shale oil exploration. The shale of the third member of the Eocene Shahejie Formation (Es_3 shales) in the Dongpu depression of the Bohai Bay Basin is dominated by clay minerals, with a non-negligible proportion of gypsum, anhydrite, and halite. They contain abundant OM with a mean total organic carbon content of 1.26 wt %. The development of salt rocks revealed the arid and transiently humid climate during the Es_3 period and an evaporating environment with a shallow lake level at the Dongpu Ancient Lake Basin. OM enrichment was synthetically affected by the palaeoenvironment during the Es_3 period. The paleolake with a paleosalinity as high as 23.43‰ was nutritious and promoted the prosperity of salt loving organisms causing high paleoproductivity.

The Es_3 shales were deposited under anoxic and dysoxic conditions in a deep lake, which provided good conditions for OM preservation. In addition, salt rocks itself are good caprocks to prevent the loss of shale oil. Under the dual guarantee of high productivity and good preservation conditions, OM is much enriched in the Es_3 shales. OM enrichment was synthetically affected by the palaeoenvironment during the Es_3 period. The horizontal difference of paleoclimate controlled the discrepancy of salinastones distribution, OM enrichment, paleosalinity, andpaleoproductivity in different saline surroundings of Dongpu Depression. The composite patterns of palaeoenvironmental variation affected the vertical anisotropic enrichment of OM. Seven stages were divided for the Es_3 period to reflect the effects of vertical anisotropy on OM enrichment. Stages I, V, and, VII deposited thick salt under an arid climate and provided a good seal-capping and preservation condition for the OM enriched in stages II, III, IV, and VI. The shale reservoirs deposited in stages III and IV were favorable for shale oil exploration.

1. Introduction

Shales interbedded with carbonates, sulfates, or chlorates have been regarded as significant source rocks for oil and gas generation in saliferous sedimentary basins, and have received considerable research attention (Sonnenberg and Pramudito, 2009; Philp and Fan, 1987; Jin et al., 2008; Cai, 2012). These sediments widely existed in the Eocene saliferous sedimentary basins of China, such as the Qianjiang Formation in the Jianghan Basin, the Shahejie Formation in the Bohai Bay Basin, and the Hetaoyuan Formation in the Nanxiang Basin (Wang et al., 1997; Li et al., 2015a,b; Wu et al., 2018). Shale sediments formed in saline environments are more favorable for organic matter (OM) enrichment

* Corresponding author. State Key Laboratory of Petroleum Resources and Prospecting, China University of Petroleum, Beijing, 102249, China.
** Corresponding author. State Key Laboratory of Petroleum Resources and Prospecting, China University of Petroleum, Beijing, 102249, China.
E-mail addresses: jfjhtb@163.com (F. Jiang), cd18801323769@163.com (D. Chen), 1123896734@qq.com (C. Zhu), 864025628@qq.com (K. Ning), lin.ma@manchester.ac.uk (L. Ma), 359329306@qq.com (T. Xu), qr96118@126.com (R. Qin), 18810599931@163.com (B. Li), cyy20110125@sina.cn (Y. Chen), 17801233378@163.com (L. Huo), 19971252151@163.com (Z. Xu).

https://doi.org/10.1016/j.petrol.2021.110035
Received 15 September 2020; Received in revised form 18 October 2021; Accepted 9 December 2021
Available online 11 December 2021

and preservation than those deposited in freshwater environments (Jin et al., 2008; Grosjean et al., 2009; Cai, 2012). The water with high salinity would present obvious stratified water column, and the reducing condition at the bottom is avail for the OM preservation (Jin et al., 2008; Cai, 2012). The representative saline shale sediments in China is the Eocene Shahejie Formation's shale reservoir in the Dongpu depression of Bohai Bay Basin. Currently, approximately 90% of the oil and gas have been discovered in the north saline region of the Dongpu depression (Ning, 2017, Fig. 1), where shale oil was discovered (Wang et al., 2015). Previous studies show that the salt distribution, OM characteristics, thermal maturity, and hydrocarbon potential present great discrepancies and vertical anisotropy in the Shahejie shale reservoir of the Dongpu depression (Wang et al., 2015; Ning, 2017). However, rare researches have been systematacially performed on the mechanism of these discrepancies and anisotropy. The salt deposition and OM enrichment are closely associated with the palaeoenvironments, paleosalinity, paleoredox conditions, occlusive-open system, and hydrothermal history, as well as their variations (Lu et al., 1993; Peters et al., 1996; Jin et al., 2008; Grosjean et al., 2009).

Dongpu depression is a momentous oil-bearing sedimentation unit in China. After more than 50 years of exploration and development, the proved oil reserves in Dongpu depression are 6.01×10^8 t with a proven degree of 48.6%, and the proved gas reserves are 1388.29×10^8 m^3 with a proven degree of 37.8% (Liu et al., 2014; Wang et al., 2020). The exploration and development of conventional oil and gas resources had made profound progress, while the exploration of unconventional oil and gas resources is still at the initial stage. Recently, shale oil resource in the Dongpu depression shows great potential with the breakthroughs in Pushen 18-1 and Wengu 4 wells in the northern (Li et al., 2013; Zhang et al., 2015; Fu, 2015).By reconstructing the palaeoenvironments and their evolutions, this study tries to explore the mechanism of anisotropy in salt and OM enrichment for the representative study area of the Dongpu depression through geological, mineralogical, and geochemical analyses. This study is essential for the understanding of the mid-latitude Eocene palaeoenvironment. It has significance for the shale oil exploration in the Dongpu depression, as well as implications for other sedimentary basins with similar features.

2. Geological setting

The Dongpu depression, located in Bohai Bay Basin of eastern China, is a crucial petroliferous unit (Chen et al., 2013; Lyu et al., 2016, Fig. 1a). The crystal basement of Dongpu depression formed from Archean to the Paleoproterozoic, and suffered a platform cover deposition from the Mesoproterozoic to the Triassic (Hou et al., 2001). From the Mesozoic, the depression began to rift continuously (Su et al., 2006). From Eocene to Oligocene, Dongpu depression rifted with NW-SE extension after the Yanshan Movement (Chen et al., 2013). Then, the depression suffered subsiding and depositing during Neogene and Quaternary (Wang et al., 2015). These tectonic movements formed the western gentle slope belt, western sub-depression, central uplift belt, eastern sub-depression eastern steep slope belt in Dongpu depression (Fig. 1a and c). These sub-depressions are segmented by central fault systems such as the Lanliao, Huanghe, and Changyuan basement faults (Lu et al., 1993; Jiang et al., 2008).

The Dongpu depression is mainly covered by Cenozoic sediments, including the Eocene Shahejie (Es) and Dongying (Ed) Formations, the Neogene Guantao (Ng) and Minghuazhen (Nm) Formations, and the Quaternary Pingyuan (Qp) Formation from bottom to top (Qi and Yang, 2010; Li et al., 2013; Zhang et al., 2015, Fig. 2). The Es have been divided into Es_3, Es_2, and Es_1 members from bottom to top (Qi and Yang, 2010, Fig. 2). The thickness of Es_3 is up to 800 m, dominated by mudstones and dark gray mudstones with interbedded salt and gypsum (Du et al., 2008, Fig. 2). Furthermore, Es_3 has been further divided into the upper (Es_3U), middle (Es_3M), and lower (Es_3L) sub-members (Fig. 2). Es_1, Es_3U, Es_3M, Es_3L, and Es_4U have been regarded as the five most crucial suit of resource rocks, where have discovered abundant shale oil since 2010 (Wang et al., 2015).The shale sediments in Es_3 member hereinafter will be referred to as Es_3 shales.

The Es_3 period was the primary rifting phase after the basic tectonic framework of the Dongpu depression formed. During this period, the Wenxi fault system exhibited relatively intense activity, and the

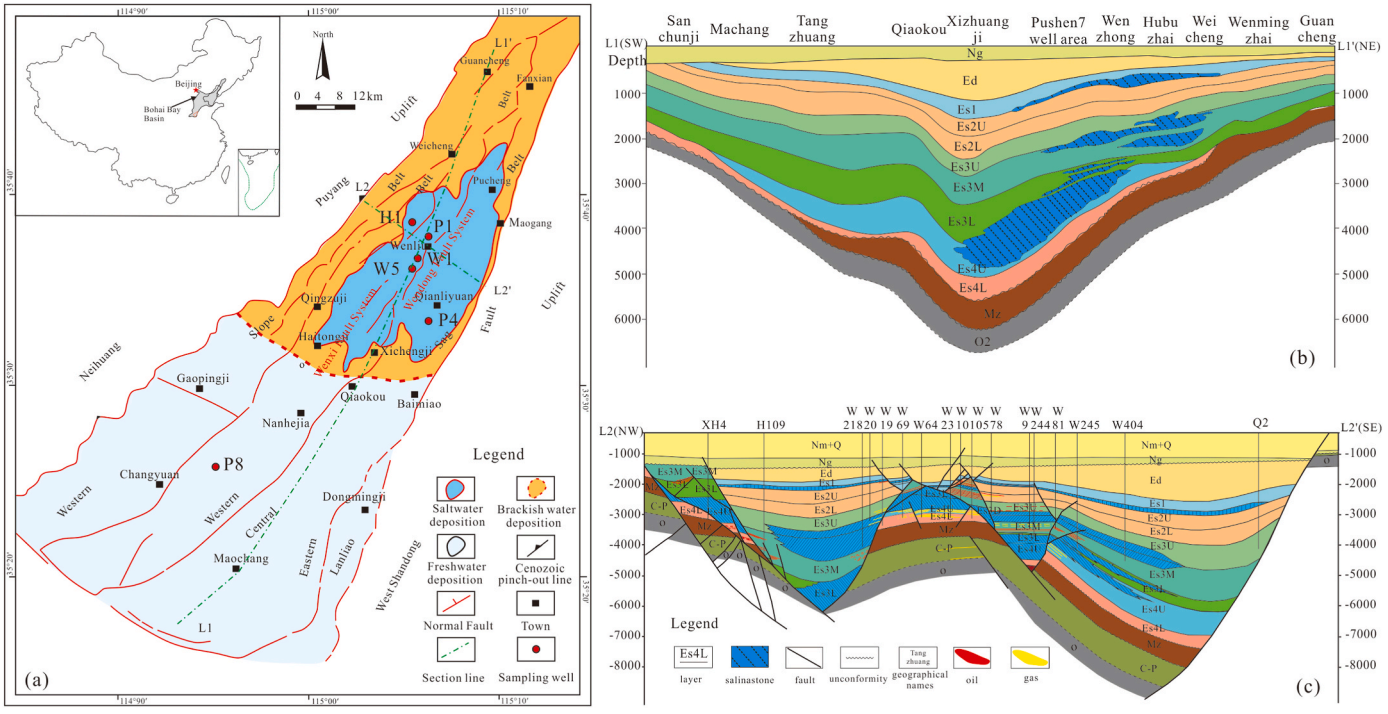

Fig. 1. Regional location of the Dongpu depression in the Bohai Bay Basin (modified after Chen et al., 2012), and the salt distribution. (a) shows the region structural map and deposited environments, and (b) is the Northeast profile, and (c) are the Southeast profile.

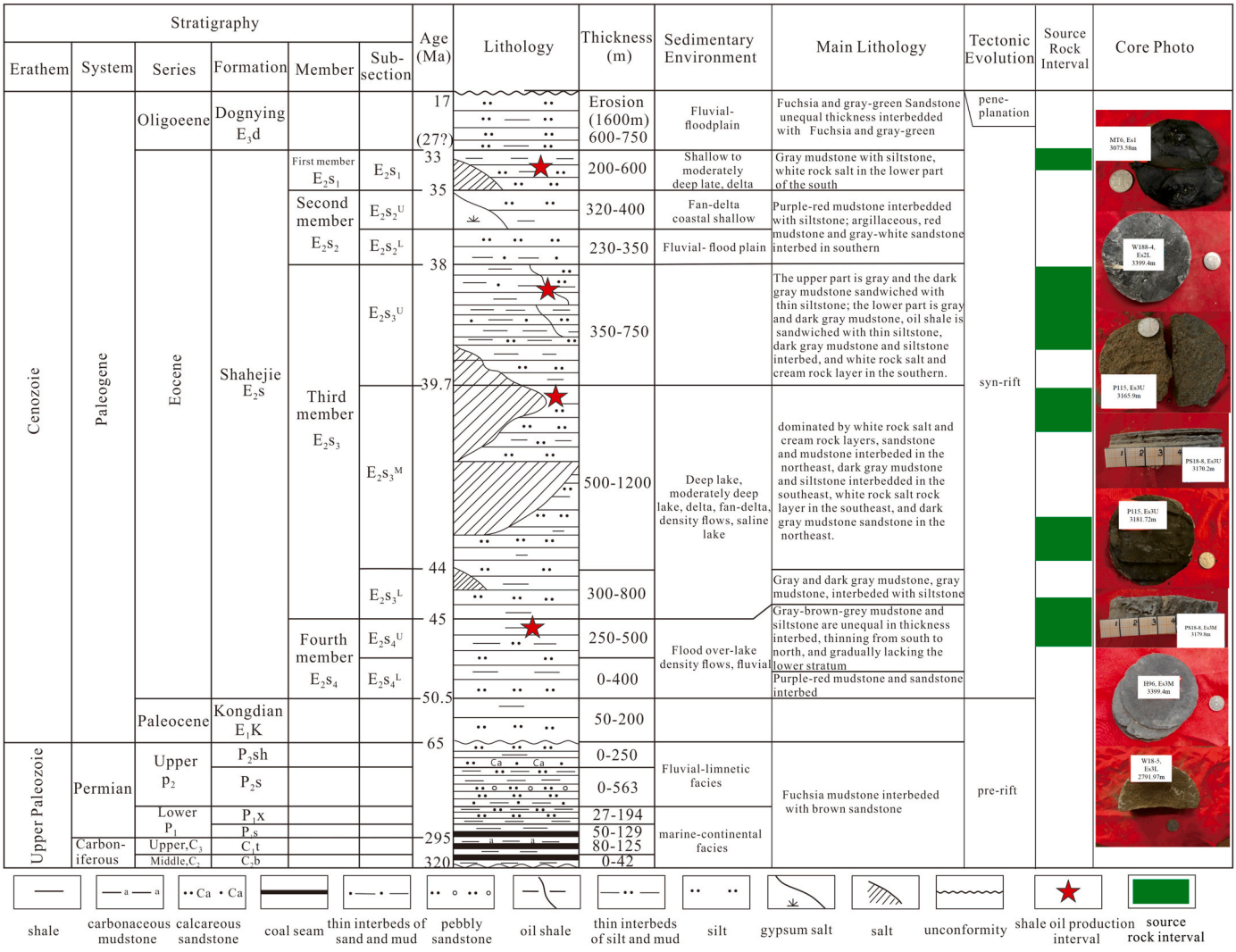

Fig. 2. Generalized stratigraphic column of the Dongpu depression in the Bohai Bay Basin and the shale oil production layers (modified after Wang et al., 2015; Zhu et al., 2021).

deposition thickness of the entire area exhibited minimal differences. In the Es_3M period, the Wendong fault system first emerged with weak activity intensity. During the later Es_3M period, the activity intensity of the Wenxi and Wendong fault systems strengthened, and the central uplift belt briefly appeared. The horst and graben north of the central uplift belt formed during the Es_3U period. As shown in Fig. 2, the depression suffered semi-deep lake, deep lake, fluvial-flood plain and deltaic environments during Eocene, and paleoclimate underwent conspicuous changing according to the lithology records. Based on the salt distribution and depositional environments, the Dongpu depression has been divided into three regions: including north saline region (SR) containing over 90% of discovered oil-gas resources, south freshwater region (FR); and brackish region (BR) in the zone (Chen et al., 2012, Fig. 1a).

3. Data and methodology

Total 36 Es_3 shale samples were used in this study to reconstruct the palaeoenvironment of Early Eocene Dongpu Depression, of which 23 samples from the SR, and 7 samples from the BR and 6 samples from the FR (Fig. 1). The lithology of these available samples includes black shales and dark gray mudstones with white salt (Fig. 2). All samples were carried out with total organic carbon (TOC) content tests, X-ray diffraction (XRD), and elemental analysis. All experiments were executed at the State Key Laboratory of Petroleum Resources and Prospecting in China University of Petroleum (Beijing). In addition, the well logging data were collected from the Sinopec Zhongyuan oilfield.

The TOC content was tested by using LECO CS230 carbon/sulfur analyzer in this study. Before experiment, powdered samples were conducted to decalcify carbonatite by treated with hydrochloric acid to (Farhaduzzaman et al., 2012; Jiang et al., 2016a).

Mineralogical analysis was performed on a Rigaku D/MAX-2000 diffractometer with 35 kV/30 mA energy and Cu K-α radiation. The slides were scanned at a 2θ value ranging from 5° to 60° with a scanning rate of 10°/min. The mineral content was semi-quantified by using the area of intensity peak of the corresponding mineral curve (Pecharsky and Zavalij, 2003).

The major elements were tested by Axios-mAX X-ray fluorescence spectroscopy (XRF) to reconstruct the palaeoenvironment. Before the experiment, the samples were ground to a powder and dried. The results were presented as the weight percent of major elements, expressed as oxides including Fe_2O_3, SiO_2, CaO, K_2O, Al_2O_3, MgO, TiO_2, Na_2O, P_2O_5, and MnO. The trace elements were measured by Thermo Electron Corporation X-7 series Inductively Coupled Plasma Mass Spectrometry (ICP-MS). The results were presented as the concentration in parts-per-million (ppm). The measured trace elements including Si, Al, Na, Ba, Sr, P, Zr, Ca, As, Cd, Cu, K, Mn, Mo, Ni, Pb, Ti, Cr, Zn, Mg, and Fe. Before the experiment, the specimens were ground to a 200 mesh and naturally

air-dried. The sample were weighed in the process of experiment to obtain the loss on ignition. The powdered samples were dissolve by using HNO_3 and HF, and then filtered and heated for 48 h under 190 °C until nearly dry. Prior to analysis, the samples were washed by using sub-boiled deionized distilled water at 150 °C. For maximum sensitivity and stability, the heavier trace elements (Th, Hf, U, and Ta) and lighter trace elements were measured separately. Other details of experiments can be referred from Li et al. (2009) and Yang et al. (2013).

4. Results

4.1. Mineral geochemistry

Shales was deposited under the low-energy environment, and underwent complex palaeoenvironmental changes (Katz and Lin, 2014; Liu et al., 2018). The abundant organic and mineral combinations in shales reflect the high-frequency climatic and environmental variations (Schieber and Zimmerle, 1998; Katz and Lin, 2014; Liu et al., 2018). The XRD analyses in this study show a wide range of inorganic compositions for the Es_3 shales in the Dongpu depression (Fig. 3). The predominant components are clay minerals ranging from 6.70 wt % to 66.50 wt % (avg. 35.66 wt %), followed by calcite (0.50–60.60 wt %, avg. 22.88 wt %), and ankerite (1.10–83 wt %, avg. 18.24 wt %). The quartz takes lower proportion of 3.40–28.30 wt % (avg. 13.25 wt %). A noticeable feature is that the salts (gypsum, anhydrite, and halite) have a non-negligible proportion with an average value of 4.08 wt % (0–18.2 wt %). The mineral composition of the Es_3 shales in the Dongpu depression have notable differences from that of the Yanchang shales in the Ordos Basin. The Yanchang shales are typical freshwater sediments and contain abundant quartz and feldspar, weak carbonate minerals, and no salt (Jiang et al., 2016a, 2016b). This result indicates that the climate was torrid and arid when Es_3 shales deposited, which is different from the moist depositional environment for the Yanchang shales deposition. The TOC content of Es_3 shales varies from 0.12 to 5.70 wt % (avg. 1.26%), which is consistent with that in Wang et al. (2015) but lower than that of the Yanchang shales (Jiang et al., 2016a) (see Fig. 4).

From the SR to the BR and FR, the contents of clay and quartz increase, but those of calcite, ankerite, salt, and TOC decrease (Figs. 3 and 6, Table 1). The decreasing salt content (yellow dotted line in Fig. 3) indicates more arid paleoclimate in the SR and relatively moist environment in the FR. Moreover, the similar trend in TOC content implies a more anoxic environment in the SR. These phenomena imply that salt is conducive to OM preservation and enrichment to some extent.

In addition, illite dominates the clay minerals for Es_3 shales with an average value of 52.81 wt %, followed by I/S (9.00–54 wt %, avg. 34.56 wt %). Illite content in the SR is abundant with an average value of 57.17 wt % (34.00–85.00 wt %), higher than those in the BR (41.00–60.00 wt %, avg. 51.14 wt %) and FR (26.00–51.00 wt %, avg. 38.00 wt %). The I/S content increases from the SR (9.00–54.00 wt %, avg. 33.13 wt %) to the FR (32.00–48.00 wt %, avg. 40.33 wt %), implying a more thermal alkaline environment in the SR.

4.2. Petrological geochemistry

Among all elements in Es_3 shales, the major elements are predominant with percentages ranging 74.12–83.86 wt % (Table 2 and Fig. 5). The contents of trace elements are slightly higher than that of the rare earth elements (REEs). The loss on ignition is non-negligible in this study. Furthermore, the contents of elements were compared and normalized to the upper continental crust (UCC) in this study to observe the difference form the average crustal composition (Taylor and McLennan, 1985; McLennan et al., 1995).

4.2.1. Major element geochemistry

According to the XRF analysis (Table 2), the contents of the major elements of Es_3 shales are 0.53–5.79 wt % for Na_2O; 0.862–3.99 wt % for K_2O; 15.66–55.71 wt % for SiO_2; 5.04–18.74 wt % for Al_2O_3; 2.25–15.12 wt % for Fe_2O_3; 0.61–14.43 wt % for MgO; 0.03–0.23 wt % for MnO; 0.20–0.80 wt % for TiO_2; and 0.07–0.25 wt % for P_2O_5. The SiO_2, Al_2O_3, and CaO have high percentages in the Es_3 shales, while the contents of Na_2O, K_2O, Fe_2O_3, MgO, MnO, TiO_2, and P_2O_5 are relatively low. The high correlation between Al_2O_3 and SiO_2 (Table 3) suggests that the primary hosts of Si are clays, which is consistent with the mineral results. Given the low content of potassium feldspar, the positive correlation of K_2O with Al_2O_3 (Table 3) indicates that illite and smectite are the main hosts for K and Al. The weak correlation between Na_2O and SiO_2 (Table 3) implies that Na does not primarily reside in feldspar and may contain salt. By contrast, Al_2O_3 shows a strong negative relationship with CaO with low deviation from the best-fit line (Table 3). This result reflects a mixture between terrigenous material and carbonates formed in the lake, and the dominant hosts of Ca are carbonate minerals. The good positive correlation between Al_2O_3 and TiO_2 (Table 3) indicates that Ti is mainly relevant with clay minerals. The low MgO content (avg. 3.57, 5.32, and 2.81 wt % in the SR, BR, and FR, respectively; Table 2) in Es_3 shales implies the minor presence of dolomite in the Dongpu depression.

Unlike the UCC, Es_3 shales enrich CaO and P_2O_5 and lose Na_2O (Fig. 5a). The contents of SiO_2, Al_2O_3, Fe_2O_3, and TiO_2 in the FR are

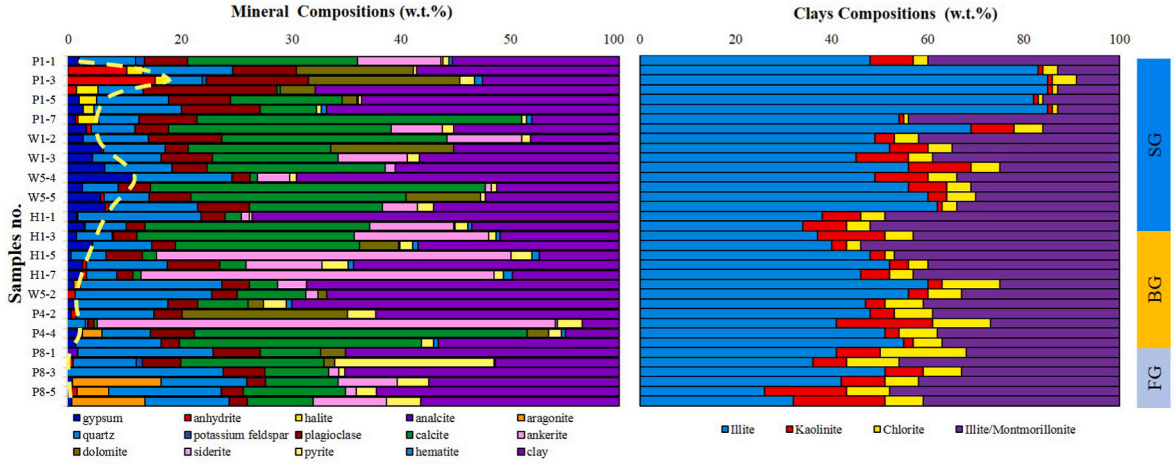

Fig. 3. Mineral composition of Es_3 shales in the Dongpu depression. SR, BR, and FR are abbreviations for the saline region, brackish region, and freshwater region, respectively. The yellow dotted line is a trend for the sum of gypsum, anhydrite, and halite, showing a decreasing trend from the SR to FR. (For interpretation of the references to colour in this figure legend, the reader is referred to the Web version of this article.)

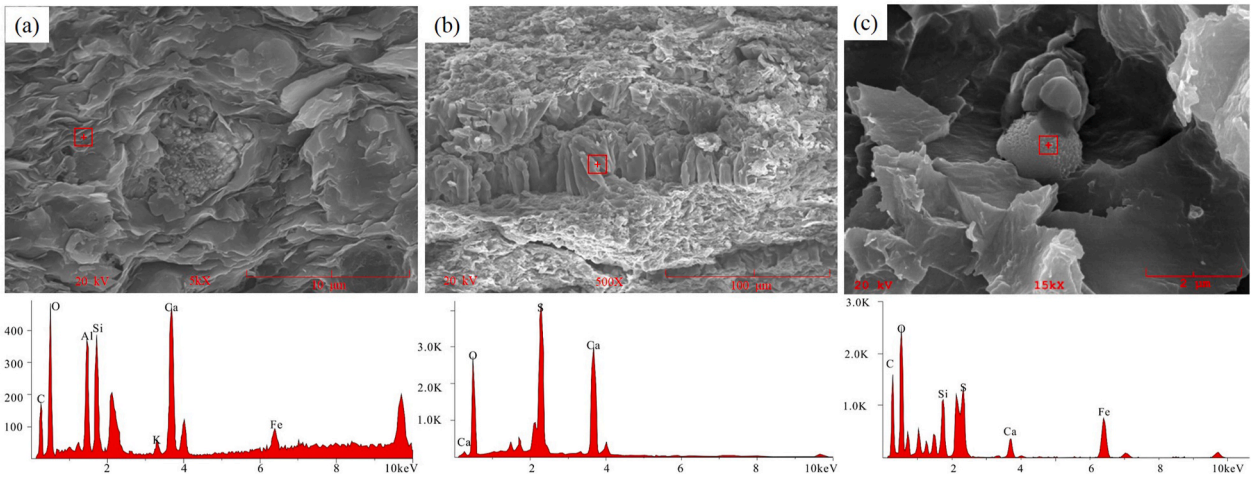

Fig. 4. Photomicrographs for Es_3 shales at 3170.2 m (a), 3885.8 m (b), and 4585.34 m (c) in the Dongpu depression. (a), (b), and (c) shows the morphology of clay mineral, gypsum and OM separately, and evidences from energy spectrum.

slightly higher than those in the SR and BR, indicating more clay minerals in the FR. This finding is consistent with that of X-ray mineral analysis. Conversely, Na_2O and CaO contents in the SR are slightly higher than those in the FR and BR, implying that the salt content in the SR is higher than those in the FR and BR.

4.2.2. Trace and REE geochemistry

The trace elements and REEs abundances in Es_3 shales are low in general (Table 2). Elements such as Hf, Ta, Co, Nb, Ni, Zr, Th, Sc, and REEs are considered to be stable during deposited processes, and can be utilized to determine the source composition of sediments in the sedimentary cycle (Taylor and McLennan, 1985; Shao et al., 2001). The shale samples in the SR, BR, and FR generally show similar distribution patterns of these trace elements and REEs (Fig. 5b and c), implying the similar provenance. In contrast to the UCC, Es_3 shales have high concentrations of trace elements, including B, Li, Cr, Ni, Mo, Cd, Sb, U, Re, and Bi, and various depletions of Be, Co, Zn, Ga, Rb, W, Tl, Nb, Ta, Zr, and Hf (Fig. 5b). The concentrations of B, Mo, U, and Re in the SR are higher than those in the BR and FR, while the concentrations of Zn, Cd, Sb, Pb, Zr, and Hf are relatively high in the FR (Fig. 5b). Most REEs contents are close to the UCC and show plant bulk REEs concentrations ($\sum REEs_{UCC}$), except the high Tb_{UCC} and low Gd_{UCC}, showing slight enrichment of REEs in Es_3 shales. The $\sum REEs_{UCC}$ in the FR is higher than those in the BR and SR overall, implying ascendant provenance and source input in the FR.

5. Discussion

5.1. Palaeoenvironment of Dongpu Ancient Lake in Es_3 period

5.1.1. Paleosalinity

The paleosalinity reconstruction is beneficial for the understanding of lake evolution and the difference of OM enrichment among the SR, BR, and FR. Numerous studies on modern and ancient sediments suggest that the salinity quantitatively relates to the adsorbed boron content in clay minerals (Curtis, 1964; Couch, 1971). This relationship between boron uptake from water and salinity can be described as (Walker and Price, 1963; Couch, 1971):

$$\log B = C_1 \log S + C_2 \quad (1)$$

where S is the salinity of water (‰), B is the boron uptake content (ppm), and $C_1 = 1.28$ and $C_2 = 0.11$ are constants.

Based on the differences in "boron-uptake ability" among various clay minerals, Couch refined the "uptake boron" by using "Kaolinite boron" according to

$$B^* = \mathrm{B} / (4X_i + 2X_m + X_k) \quad (2)$$

where B^* is the "kaolinite boron" (ppm), which represents the boron adsorbed in clay minerals; X_i, X_m, and X_k are the weight fractions of illite, montmorillonite, and kaolinite, respectively; and B is the measured boron concentration (ppm).

Combining with the contents of clay minerals acquired from XRD analysis, the calibrated boron concentration and paleosalinity of the Dongpu Ancient Lake in the Es_3 period can be calculated (Fig. 6). The paleosalinity in the SR ranges from 3.94‰ to 23.43‰ with an average of 10.84‰, which is higher than those in the BR (6.79–14.80‰, avg. 9.40‰) and FR (6.43–10.55‰, avg. 8.99‰; Fig. 6). The paleosalinity decreases from the SR to FR, similar to the measured and calibrated boron (Fig. 6 and b). The calibrated boron is lower than the measured boron, and shows positive relationship with it (Figs. 6 and 7b). These results suggest that it is necessary to rectify the boron concentration before paleosalinity calculation. TOC first increases with paleosalinity and then decreases (Fig. 7a). The paleosalinity of high TOC abundance samples (TOC >2.0 wt %) ranges from 7.39‰ to 12.71‰, indicating the most favorable paleosalinity for OM enrichment. In contrast, TOC is less than 1% until paleosalinity is greater than 23.14‰ (Fig. 7a).

In addition, the paleosalinity interpretations could also be cross-checked by other independent paleosalimeters, including B*/Ga, Sr/Ba, Rb/K, Sr/Ca, and Ca/(Ca + Fe) ratios (Chivas et al., 1986; Deckker et al., 1988; Scheffler et al., 2003; Song, 2005; Wang et al., 2006; Ye et al., 2016; Liu et al., 2018). These elemental ratios are high in saline water and low in freshwater The variations of B*/Ga, Sr/Ba, Rb/K, and Sr/Ca have good comparability with Couch's paleosalinity, especially for the B*/Ga value (Fig. 8). This fluctuation in paleosalinity is also in response to the climate change during the Es_3 period for the Dongpu depression.

5.1.2. Paleoclimate and relative lake level

Paleoclimate has a significant influence on the composition of paleolakes, including weathering processes, freshwater inflow, lake level, salinity, and biolimiting materials (Sun et al., 2016; Yan and Zheng, 2015). Climatic variation can be inferred from the discrimination diagrams of major and trace elements ratios, including Rb/Sr, Sr/Cu, and Ga/Rb (Song, 2005; Liu et al., 2018; Roy and Roser, 2013).

Sr/Cu is a good proxy for tracking the paleoclimate (Learman et al., 1989). Its value of 1.3–5.0 suggests humid climate, and >5.0 indicates xerothermic environment. For terrestrial sediments in China, Sr/Cu > 10 indicates xerothermic conditions, and the range of 1–10 indicates humid conditions (Song, 2005; Liu and Zhou, 2007). Considering the

Table 1
Main mineral compositions of the Es_3 shales in the Dongpu depression. Note: SR, BR and FR are abbreviation for the saline region, brackish region, and freshwater region, respectively. Salt means the sum of gypsum, anhydrite, and halite. I/S is the Illite and Smectite mixed layer.

Region Min-Max, Mean	TOC, wt. %	Clay, wt. %	Calcite, wt. %	Ankerite, wt. %	Quartz, wt. %	Plagioclase, wt. %	Salt, wt. %	Clay minerals			
								Illite wt. %	Kaolinite wt. %	Chlorite wt. %	I/S wt. %
Whole	0.12–5.70, 1.26	6.70–66.50, 35.66	0.50–60.60, 22.88	1.10–83.00, 18.24	3.40–28.30, 13.25	1.10–24.30, 4.08	0–18.20, 4.08	26.00–85.00, 52.81	1.00–20.00, 6.69	1.00–18.00, 5.94	9.00–54.00, 34.56
SR	0.39–5.70, 1.59	14.30–66.50, 34.15	0.50–60.60, 25.33	1.10–63.90, 18.95	5.50–22.30, 11.03	2.90–24.30, 8.66	0.80–18.20, 5.70	34.00–85.00, 57.17	1.00–14.00, 5.70	1.00–6.00, 4.00	9.00–54.00, 33.13
BR	0.12–1.85, 0.64	6.70–59.30, 37.44	0.60–60.20, 21.87	2.20–83.00, 30.13	3.40–25.50, 15.44	1.10–8.00, 4.89	0–2.80, 1.56	41.00–60.00, 51.14	2.00–20.00, 5.86	6.00–12.00, 8.71	25.00–41.00, 34.29
FR	0.25–1.22, 0.75	22.40–49.70, 39.33	11.00–26.00, 15.33	1.90–13.30, 6.98	11.50–28.30, 19.22	3.30–8.5, 5.62	0–1.90, 0.83	26.00–51.00, 38.00	7.00–19.00, 11.40	7.00–18.00, 10.17	32.00–48.00, 40.33

small scale of Dongpu Ancient Lake in the Es_3 period, Sr/Cu ratio is more sensitive to climatic variation. In this study, the average value of Sr/Cu is 63.63 (6.49–243.83, Table 4), implying an arid subtropical climate in the Es_3 period for the Dongpu depression, which is similar to the Eocene Hetaoyuan period of the Biyang depression (Wang et al., 1997).

Rb/Sr could also be used as an alternative indicator of paleoclimate. Its value could reflect the weathering condition, sedimentary provenance, and granularity (Huang et al., 2007; Sun et al., 2010). Low Rb/Sr value suggests dry climate adverse to chemical weathering, whereas the high Rb/Sr value indicates warm-wet climate facilitating intense weathering (Roy and Roser, 2013; Liu et al., 2018). In this study, relatively high Sr/Cu and low Rb/Sr values of SR Es_3 shale samples imply drier climate in the SR than those in BR and FR during Es_3 period.

Lake water level is associated with climate and strongly influences palaeobios groups in paleowater (Liu et al., 2018). Rb/k and Mn/Fe ratios are two powerful proxies for reflecting the water depth of paleolakes (Xiong and Xiao, 2011; Liu et al., 2018). Rubidium is more easily absorbed by clay minerals and transported to far distances and into deep lakes. Therefore, the Rb/k value is relatively high in deeper water sediments. Fe deposits with colloform, and is usually found in near-shore and shallow-water settings. While, Mn exists in normal lake water as Mn^{2+} and concentrates in the far and deep portions of a lake. These phenomena lead to a high Mn/Fe value in deep water sediments. In this study, the Rb/k and Mn/Fe values in the SR are higher than those in the FR (Table 4), implying the relatively deep water level in the SR. In contrast, the Rb/k and Mn/Fe values in the BR are the highest, which may be attributed to the structure factor. The BR locates at the lowest position of Dongpu depression, and the SR on the North Slope (Fig. 1b), which are the results of faulting activity.

The sources of Ti, Al, and Zr are the inorganic debris incorporated into terrigenous sediments, which are highly insoluble in surface water (Drexler et al., 2014). High values of these elements indicate that abundant terrestrial matter had been transferred into the lake. The values of these elements decrease from the FR to the BR and SR, thereby indicating provenance direction from south to north (Table 4; Fig. 1a and b).

5.1.3. Redox conditions

Redox conditions are critical to OM preservation and the quality of source rocks in sedimentary basins. Redox-sensitive metal elements, including V, Mn, Ni, Re, Mo, and U, were highly enriched in various geological setting and involved in shale sediments (Piper, 1994). These elements have been widely used to track the redox environment during deposition (Piper, 1994; Schröder and Grotzinger, 2007).

The source of uranium in the sedimentary basin is the river sediments (Klinkhammer and Palmer, 1991). The uranium diffusing in pore waters always precipitates under an organic-rich environment (Jiang et al., 2006). The redox reaction $UO_{2(s)} + 2HCO_{3(aq)}^{-} \rightarrow UO_2(CO_3)_{2(aq)}^{2-} + 2e^{-} + 2H_{(aq)}^{+}$ always occurs under reduction (Piper, 1994). Uranium elements are immobilized in sediments due to the diffusion, reduction, adsorption, and precipitation (Klinkhammer and Palmer, 1991; Schröder and Grotzinger, 2007). Index $\delta U = 2U/(U + Th/3)$ has been used to trace the redox conditions of sediments, and $\delta U > 1$ suggests a hypoxic environment, while $\delta U < 1$ reflects a normal marine environment (Jones and Manning, 1994; Yan et al., 2015). In this study, the δU values range from 0.83 to 1.53 with an average of 1.18 in the SR, which is higher than those in the BR (0.72–1.23, avg. 1.00) and FR (0.80–1.28, avg. 0.98) (Fig. 9b). This result implies anoxic condition in the SR, dysoxic (conditions varying between anoxic and oxic) condition in the BR, and oxic condition in the FR (Wignall and Myers, 1988).

Thorium is largely independent in the grain size and clays and relatively immobile in the low-temperature surface environment, and is typically used to distinguish detrital input (Schröder and Grotzinger, 2007). The U/Th values of almost all Es_3 shale samples are less than one, indicating regular waterborne deposits with no hydrothermal input (Wu et al., 1999, Fig. 9a). Thus, most proxies of paleoredox conditions

Table 2
Comparison of major, trace, and rare earth elemental compositions of the Es_3 shales of different environments in the Dongpu depression.

ELE (ppm)	SR			BR			FR			ELE	SR			BR			FR		
	Min	Max	Mean	Min	Max	Mean	Max	Min	Mean	(ppm)	Min	Max	Mean	Min	Max	Mean	Min	Max	Mean
B	44.20	242.00	99.01	53.70	136.00	88.57	87.00	26.20	65.93	La	13.60	57.50	31.77	16.10	53.70	35.21	30.10	48.60	39.37
Li	32.10	132.00	51.93	34.90	75.50	53.11	58.20	11.90	42.12	Ce	24.70	107.00	58.66	29.80	97.10	64.33	54.00	91.30	72.65
Be	1.61	3.75	1.93	1.23	3.46	2.28	2.80	0.82	2.20	Pr	2.89	12.20	6.94	3.63	11.20	7.50	6.28	10.90	8.49
V	46.40	125.00	69.05	42.80	107.00	76.33	104.00	26.10	71.53	Nd	11.10	45.30	26.18	13.60	40.20	28.11	23.00	42.10	31.93
Cr	55.60	143.00	71.20	46.50	141.00	96.66	167.00	33.20	91.68	Sm	1.90	7.45	4.66	2.53	6.95	5.01	3.97	7.68	5.61
Co	8.50	20.50	12.46	6.58	16.70	10.96	23.00	6.69	13.95	Eu	0.34	1.45	0.94	0.48	1.55	1.09	0.75	1.52	1.13
Ni	23.80	55.60	33.04	18.70	67.30	39.43	49.30	20.60	35.38	Gd	0.30	1.09	0.69	0.40	1.04	0.76	0.55	1.13	0.84
Cu	10.90	40.70	23.54	7.62	42.70	19.27	55.40	14.90	24.98	Tb	1.56	6.10	3.92	2.24	5.77	4.26	3.21	6.63	4.77
Zn	38.70	124.00	44.86	30.70	75.80	54.13	159.00	14.70	87.18	Dy	1.45	5.55	3.49	2.00	5.17	3.78	2.95	5.50	4.18
Ga	12.80	24.50	14.15	6.76	24.10	15.67	22.00	6.07	16.72	Ho	0.30	1.14	0.70	0.41	1.05	0.76	0.58	1.06	0.82
Rb	67.80	158.00	85.97	47.00	166.00	107.31	142.00	34.90	99.87	Er	0.84	3.23	1.91	1.10	2.90	2.06	1.61	2.78	2.26
Sr	323.00	3189.00	1264.26	246.00	1858.00	894.71	1881.00	217.00	995.50	Tm	0.15	0.60	0.34	0.19	0.53	0.38	0.30	0.48	0.40
Mo	1.49	30.40	10.25	0.78	5.24	2.25	9.59	1.13	3.65	Yb	0.93	3.94	2.17	1.21	3.33	2.32	1.96	3.22	2.57
Cd	0.14	0.39	0.19	0.09	0.28	0.15	0.89	0.09	0.28	Lu	0.13	0.55	0.31	0.19	0.49	0.33	0.30	0.46	0.38
In	0.04	0.10	0.05	0.03	0.10	0.06	0.09	0.02	0.06	Y	8.49	31.90	20.10	11.60	30.10	22.11	16.60	31.00	24.08
Sb	0.76	1.70	1.04	0.50	2.23	0.99	3.51	0.39	1.56	Sc	4.00	15.60	10.05	5.62	16.20	11.33	8.23	16.10	11.43
Cs	4.71	11.90	6.15	3.13	12.20	7.46	9.69	2.34	6.59	*Na_2O	0.66	5.79	1.87	0.53	1.66	1.00	0.68	1.26	0.94
Ba	390.00	1323.00	550.83	239.00	1082.00	429.43	1363.00	225.00	608.50	*K_2O	0.86	3.78	2.10	1.08	3.99	2.57	1.90	3.51	2.47
Th	7.57	15.50	9.22	4.43	17.50	10.41	14.20	4.03	11.19	*SiO_2	18.49	55.25	32.26	15.66	54.80	35.63	34.30	55.71	42.88
U	3.07	10.40	4.63	2.00	4.92	3.31	5.60	1.74	3.63	*Al_2O_3	5.14	18.74	10.71	5.04	17.54	11.62	11.56	16.59	13.21
W	0.32	1.89	1.16	0.74	2.14	1.35	1.94	0.46	1.26	*Fe_2O_3	2.25	15.12	4.49	2.32	6.11	4.32	4.19	13.08	6.17
Re	0.00	0.02	0.01	0.00	0.01	0.01	0.01	0.00	0.00	*MgO	0.61	12.28	3.57	1.61	14.43	5.32	1.66	3.77	2.81
Tl	0.33	1.55	0.67	0.34	1.29	0.63	0.72	0.25	0.50	*CaO	2.43	30.48	16.80	3.16	25.99	15.43	5.98	17.43	12.13
Pb	14.10	33.50	19.97	7.54	30.50	16.83	79.30	12.80	34.57	*MnO	0.03	0.15	0.08	0.04	0.23	0.10	0.04	0.10	0.08
Bi	0.13	0.49	0.29	0.14	0.48	0.30	0.44	0.10	0.29	*TiO_2	0.22	0.71	0.41	0.20	0.80	0.47	0.46	0.72	0.56
Nb	4.35	15.80	9.32	5.16	18.40	11.08	16.40	4.72	11.85	*P_2O_5	0.07	0.24	0.15	0.13	0.20	0.15	0.12	0.25	0.15
Zr	88.40	178.00	89.26	50.20	186.00	103.10	930.30	50.50	262.78	*LOI	10.88	31.89	21.78	8.95	34.00	19.90	10.73	19.75	14.29
Hf	2.53	5.05	2.60	1.39	5.27	2.94	5.14	1.44	3.47										

*Note: ELE means elements; LOI is loss on ignition; SR, BR and FR are abbreviation for saline region, brackish region and freshwater region, respectively. The unit of elements marked * is wt. %, and no-marked * is ppm.

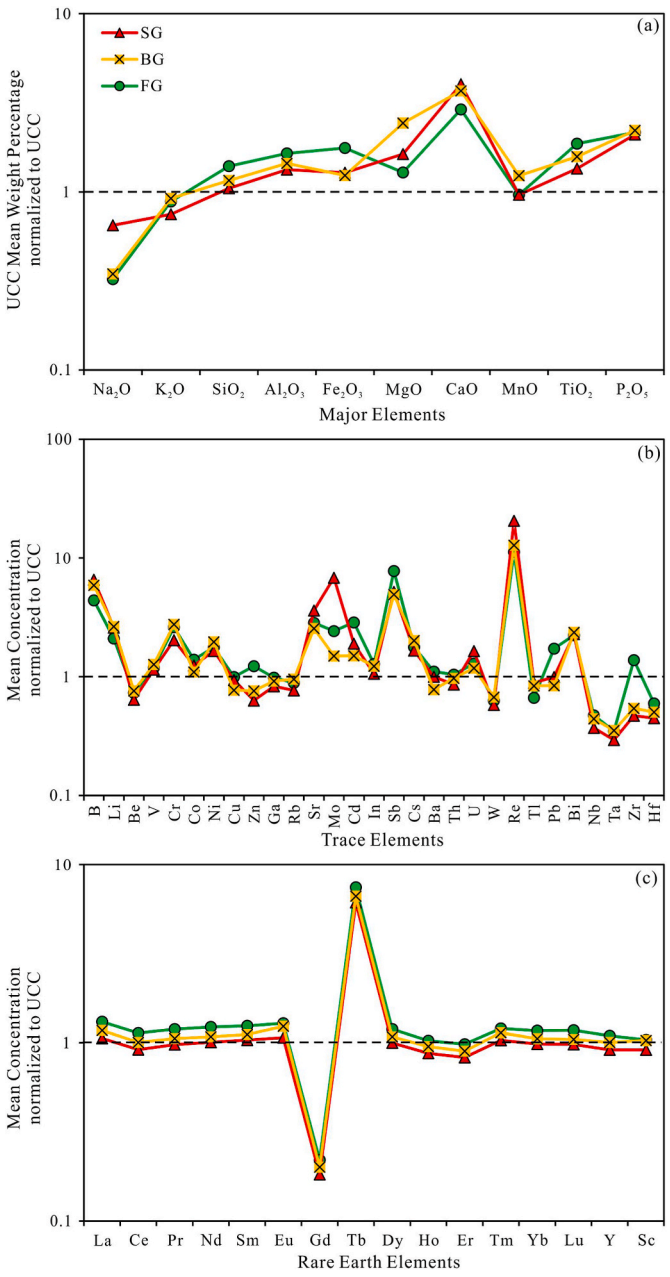

Fig. 5. Major elements (a), trace elements (b), and rare earth elements (REEs), (c) profiles of the Es_3 shales in the Dongpu depression. The content of the elements has been normalized to the UCC (Taylor and McLennan, 1985). The mean value less than 1 indicates a deletion with respect to the UCC.

consisting of the critical trace elements such as V/[V + Ni], V/Cr, and Ni/Co could be utilized to the Es_3 shales in this study (Steiner et al., 2001). The U/Th values in the SR (0.24–1.09, avg. 0.53) are larger than those in the BR (0.19–0.54, avg. 0.35) and FR (0.22–0.59, avg. 0.34). This apparent phenomenon indicates the anoxic condition in the SR, dysoxic condition in the BR, and oxic condition in the FR, which supports the analysis result of δU.

Re/Mo ratio is also considered an indicator for distinguishing redox conditions during sedimentation (Crusius et al., 1996; Lipinski et al., 2003). Because of the preferential enrichment of Re over Mo in a low-sulfide environment (Lipinski et al., 2003), high Re/Mo value suggests suboxic conditions (9×10^{-3} in the Japan Sea and 19×10^{-3} in the Arabian Sea). The low Re/Mo value reflects the anoxic or sulfidic condition considering of the low value of 0.8×10^{-3} in recent seawater (e.g., 1.5×10^{-3} in the Black Sea). For Dongpu depression, the Re/Mo value ranges from 0.26 to 3.54 with an average of 1.02 in the SR, which is close to 1.5×10^{-3} in recent anoxic sediments from the Black Sea (Lipinski et al., 2003), implying relatively oxygen-deficient conditions in the BR (Fig. 9b).

Given the comprehensive consideration of the above analysis, several appointments were set to distinguish the redox environment during the Es_3 depositional period (Fig. 9). In this study, Re/Mo value $< 2 \times 10^{-3}$ and $\delta U > 1$ indicate anoxic and sulfidic conditions; $2 \times 10^{-3} <$ Re/Mo value $< 4 \times 10^{-3}$ and $\delta U > 1$ denote dysoxic condition; $2 \times 10^{-3} <$ Re/Mo value $< 4 \times 10^{-3}$ and $\delta U < 1$ indicate suboxic condition; and Re/Mo value $> 4 \times 10^{-3}$ and $\delta U < 1$ indicate oxic condition. According to these appointments, the paleoredox environment during the Es_3 depositional period contains several alternant intervals of anoxic and oxic conditions (Fig. 10), crosschecked by other paleoredox indicators. The high U/Th, V/Th, and Mo/Th values indicate anoxic and euxinic conditions, while their low values suggest the suboxic and oxic conditions (Schröder and Grotzinger, 2007). The variations of these indexes are indeed and consistent with the change of paleoredox conditions. The redox condition of Es_3 depositional period was mainly dysoxic and anoxic, and further could be divided into seven stages in this study (Fig. 10).

The anoxic condition is beneficial for OM preservation in shale sediments. δU has a positive correlation with TOC for Es_3 shales (Fig. 9c), while the Re/Mo ratio shows a negative correlation with TOC (Fig. 9d). Moreover, the TOC contents in the BR and FR are lower than those in the SR (Fig. 6). These phenomena demonstrate the OM enrichment and preservation preference for anoxic environments.

5.2. Paleoproductivity

OM enrichment depends on the paleoproductivity of paleolake (Mayer and Schwark, 1999; Ishiwatari et al., 2005). Paleoproductivity reconstruction of Dongpu Ancient Lake during the Es_3 period is vital for estimating the OM accumulation. Previous studies of paleoproductivity mainly focus on marine environments (Henderson, 2002; Morel and Price, 2003; Paytan and Griffith, 2007), scarce for lacustrine sediments. Generally, the contribution of organisms to OM accumulation in the marine environment is lower than that in the lacustrine environment (Li et al., 2002; Ishiwatari et al., 2009). For marine sediments, Müller and Suess (1979) established a method to estimate primary productivity based on the surface sediments of the Pacific and Atlantic Oceans and the Baltic Sea. Considering the difference of the primary productivity between terrestrial and marine sediments, Li et al. (2002) investigated many current rift lakes in the Yunnan Province of China, including Dian, Erhai, and Fuxian, and derived a method to calculate the primary productivity in the rifting lakes. The equation is as follows:

$$P = \%C \times \rho \times (1 - \Phi) \,/\, \left(0.00421 \times S^{0.0826}\right) \quad (3)$$

where P is the productivity ($gCm^{-2}\ year^{-1}$); %C is the TOC content in the sediment; ρ is the dry bulk density ($g\ cm^{-3}$). Φ denotes the porosities (%). S represents the sedimentation rate ($cm\ kyr^{-1}$), calculated using the thickness and deposited time in Fig. 2.

This method has been used to calculate the Eocene paleoproductivity in the Zhanhua and Dongying depressions of the Bohai Bay Basin, and obtained good effectiveness (Liu and Xu, 2002). Given the typical features of rift lakes in the Dongpu depression (Chen et al., 2013), this method is more suitable for calculating the primary productivity of Es_3 sediments in this study (Fig. 11). The P values range from 189.17 to 2408.59 $gCm^{-2}\ year^{-1}$ with an average of 707.67 $gCm^{-2}\ year^{-1}$ in the SR, 56.12–947.24 $gCm^{-2}\ year^{-1}$ (avg. 301.20 $gCm^{-2}\ year^{-1}$) in the BR, and 108.63–610.53 $gCm^{-2}\ year^{-1}$ (avg. 370.71 $gCm^{-2}\ year^{-1}$) in the FR. On the whole, the paleoproductivity in the SR is higher than those in the BR and FR (Fig. 11a), suggesting that the high salinity is beneficial to nutrients. Moreover, the positive relationship between

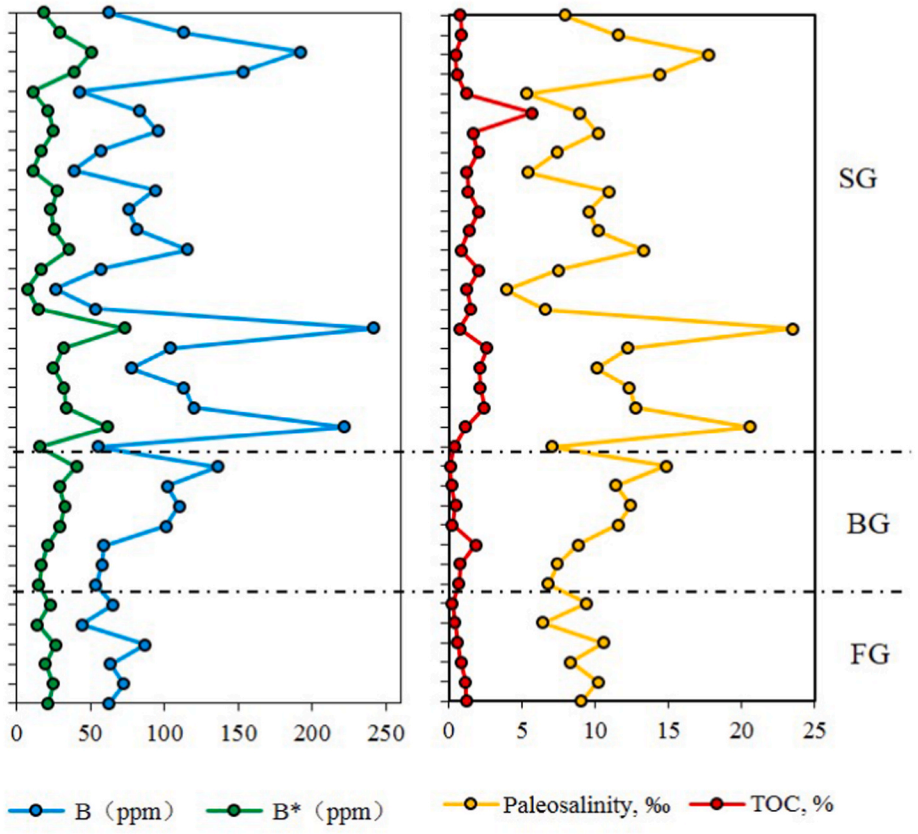

Fig. 6. Profile of boron content, paleosalinity and TOC for the Es_3 shale samples in the Dongpu depression.

Table 3
Correlation matrix of TOC and major elements for Es_3 shales.

Correlation coefficient	TOC	Na_2O	K_2O	SiO_2	Al_2O_3	Fe_2O_3	MgO	CaO	MnO	TiO_2	P_2O_5
TOC	1.00										
Na_2O	0.12	1.00									
K_2O	−0.39	0.24	1.00								
SiO_2	−0.30	0.31	0.86	1.00							
Al_2O_3	−0.30	0.34	0.95	0.95	1.00						
Fe_2O_3	−0.23	−0.06	0.12	0.11	0.10	1.00					
MgO	−0.01	−0.28	−0.28	−0.48	−0.42	−0.24	1.00				
CaO	0.28	−0.39	−0.88	−0.89	−0.91	−0.28	0.21	1.00			
MnO	−0.10	−0.38	−0.34	−0.41	−0.41	−0.18	0.48	0.40	1.00		
TiO_2	−0.38	0.31	0.93	0.96	0.98	0.15	−0.40	−0.91	−0.45	1.00	
P_2O_5	0.21	0.20	0.17	0.20	0.18	−0.25	0.13	−0.22	−0.16	0.19	1.00

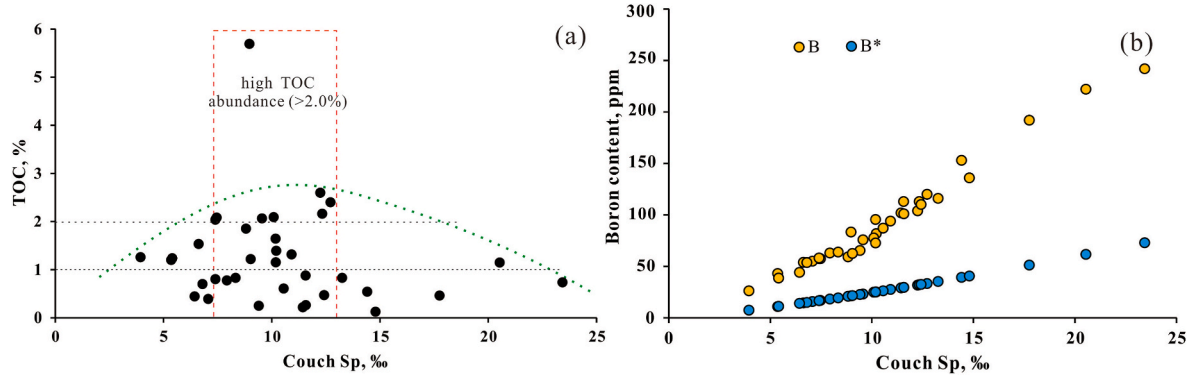

Fig. 7. Relationships among TOC, boron content, and salinity. (a) shows TOC vs. salinity, and (b) boron content vs. salinity. B* is the calibrated boron (ppm), and Couch Sp means paleosalinity calculated by Couch's method.

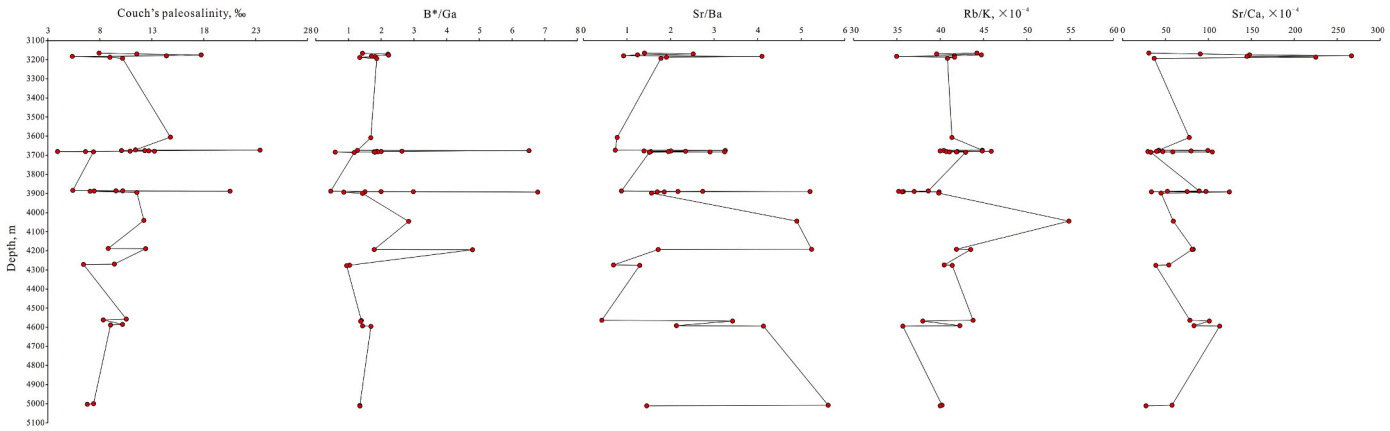

Fig. 8. Profile of salinity fluctuation for the Es_3 lake in the Dongpu depression.

Table 4
Comparison of elemental compositions of Es_3 shales in the Dongpu depression.

Indicator	Sr/Cu	Rb/Sr	Rb/k × 10^{-4}	Mn/Fe × 10^{-3}	Zr, ppm	Al, ppm	Ti, ppm
Indication	Paleoclimate	Paleoclimate	Water level	Water level	Provenance	Provenance	Provenance
SR	10.59–181.19	0.01–0.67	34.97–54.86	1.7–54.22	50.00–178.00	5.14–18.74	0.22–0.71
	88.49	0.13	41.06	21.35	89.26	10.71	0.41
BR	6.49–243.83	0.03–0.67	39.83–44.86	6.72–40.76	50.20–186.00	5.04–17.54	0.20–0.80
	85.94	0.27	41.66	24.85	103.1	11.62	0.47
FR	10.70–172.57	0.04–0.44	35.68–43.80	7.72–18.38	88.40–930.30	11.56–16.59	0.46–0.72
	62.27	0.16	40.26	13.86	262.78	13.21	0.56
Whole	6.49–243.83	0.01–0.67	34.97–54.86	1.65–54.22	50.20–930.3	5.04–18.74	0.20–0.80
	63.62	0.16	41.04	20.78	120.87	11.30	0.44

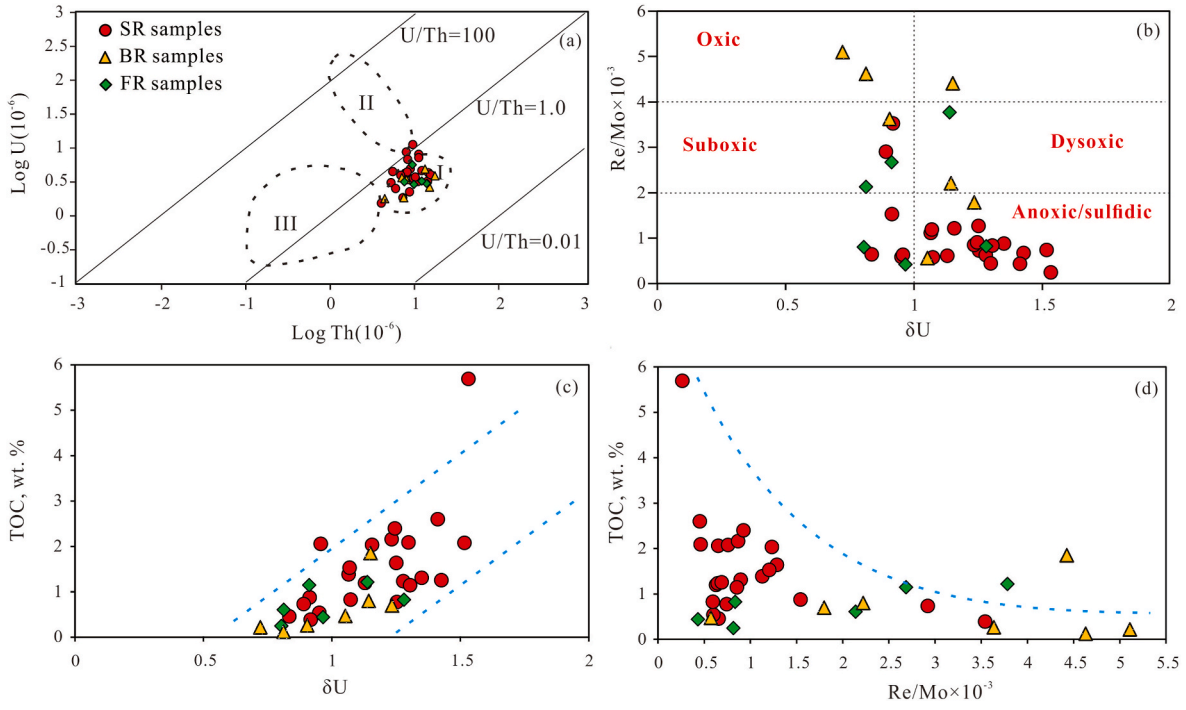

Fig. 9. Relationship between U and Th for Es_3 samples; zone I means normal ocean depositions, zone II means Pacific uplift sediments, and zone III for ancient thermal flow depositions (Wu et al., 1999). (b–d) show the cross plots of Re/Mo ratio vs. δU (b), δU vs. TOC (c), Re/Mo ratio vs. TOC (d) for Es_3 shales in the Dongpu depression.

paleoproductivity and TOC content indicates that high productivity is conducive to OM enrichment.

In addition, previous studies found that dinoflagellates, cyanobacteria, and coccolithophores have high concentrations in SR Es_3 shale sediments (Du et al., 2008; Chen et al., 2012). These micro-planktonic algae prefer the saline environment, and are the best

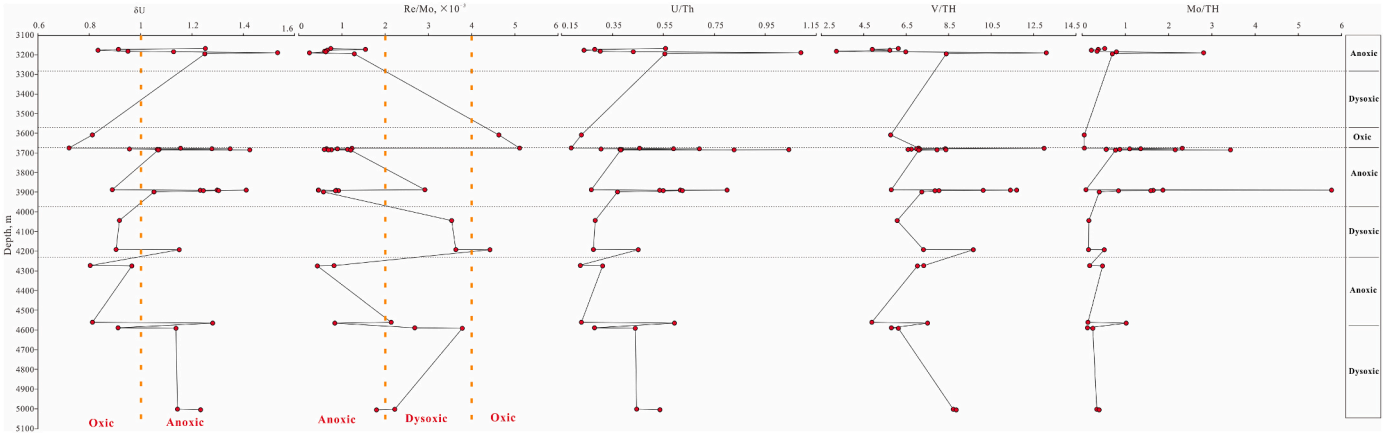

Fig. 10. Profile of redox condition fluctuation for Es_3 shales of the Dongpu depression.

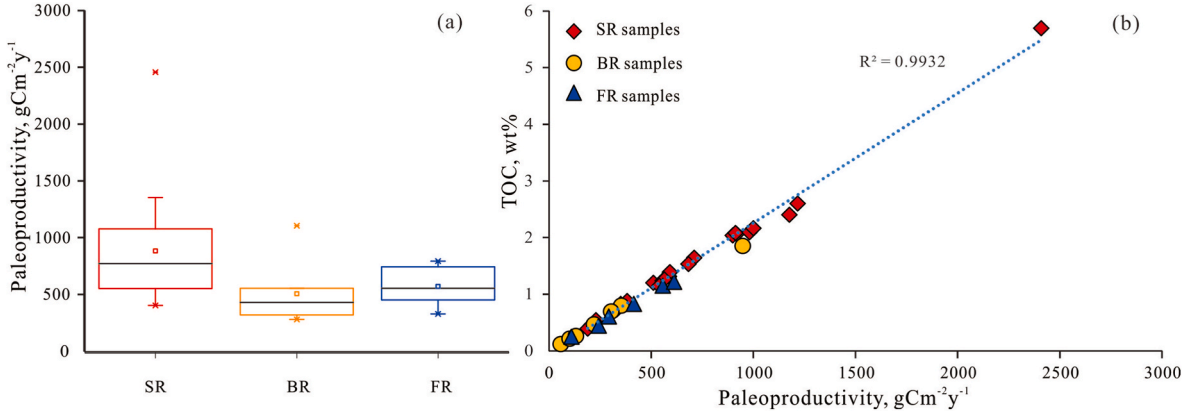

Fig. 11. Results of paleoproductivity (a) and their relationship with TOC (b) for Es_3 shales in Dongpu depression.

original parent material for petroleum generation (Petersen and Nytoft, 2006; Dutta et al., 2011). Dinoflagellates contain up to 5–36% fat which was the primary OM source, and thrive at certain salinity levels (Bao, 2009). These micro-planktonic algae have high paleoproductivities up to 3120 gCm^{-2} $year^{-1}$ for the coccolithophores (Li et al., 2014). Therefore, the saline environment is beneficial for OM enrichment.

5.3. *Effect of palaeoenvironment on OM enrichment*

OM enrichment is a complicated process, and is influenced by source,

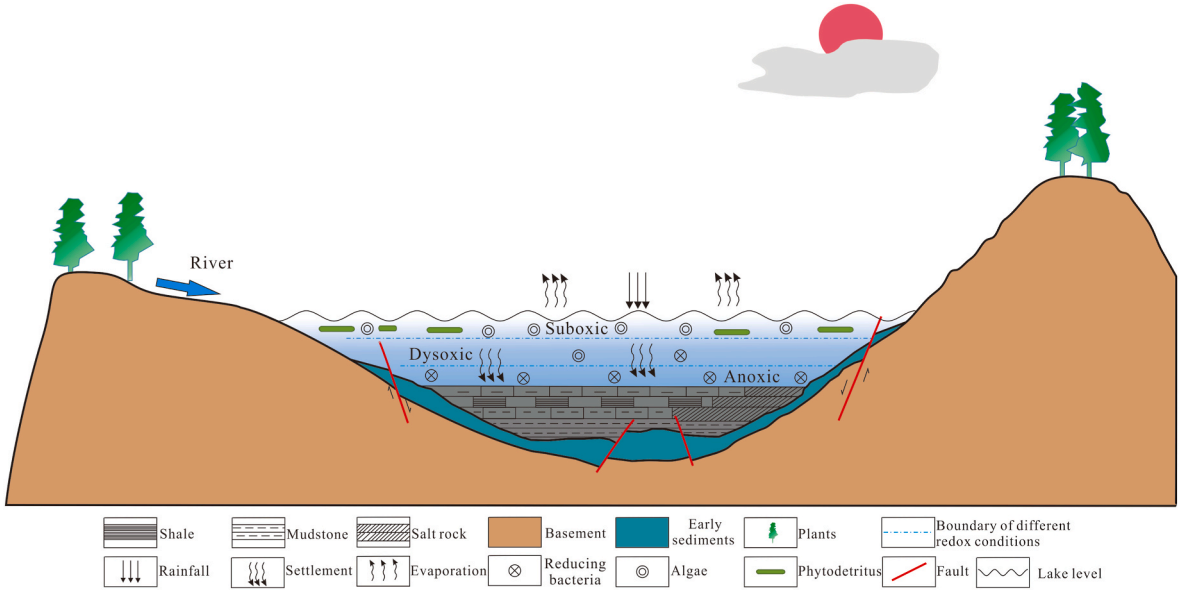

Fig. 12. Sketch illustrating the palaeoenvironment and organic matter accumulation model of Dongpu Ancient Lake at Es_3 period.

deposition, and preservation (Dean et al., 1997; Zhang et al., 2007; Li et al., 2013). The Dongpu depression suffered an arid evaporating environment during the Es_3 period (Fig. 12), leading to plenty of salt and carbonate deposition (Fig. 13a). The arid climate facilitate the high salinity in the paleolake which caused a stratified water column (Dean et al., 1997; Stow et al., 2001; Zhang et al., 2007, Figs. 12 and 13b). The reducing conditions at the bottom of the stratified water column in the SR and BR with high lake levels, is conducive to OM enrichment and preservation (Zhang et al., 2007; Li et al., 2013, Figs. 12 and 13c). Furthermore, the degree of salinity had considerable influence on productivity which may affect the OM types and amounts of palaeobios (Pedersen and Calvert, 1990; Hao et al., 2011, Fig. 13d and e). It would form the stratiform difference of palaeobios in the stratified water column (Dean et al., 1997; Stow et al., 2001; Hao et al., 2011; Li et al., 2013, Fig. 12).

In contrast, the different thicknesses of the salt layers in the Es_3 member further reflect the climate change during the Es_3 period (Fig. 2). The fluctuation of the paleoclimate affects the nutrient supply, biological types, paleosalinity, and paleoproductivity. Therefore, the vertical composite patterns of palaeoenvironmental crucially influence on the anisotropy of OM enrichment, which need further discuss.

5.4. Palaeoenvironmental evolution and its effect on OM enrichment

The Palaeoenvironments during Es_3 period in the SG, BG, and FG present obviously horizontal differences, and they evidently influence on the anisotropy of OM enrichment. While, the vertical variation of palaeoenvironments and their assemblages also affect the vertical anisotropy of shale sediments and OM enrichment. In this study, a high-resolution evolution profile of the palaeoenvironment during Es_3 period was reestablished (Fig. 14). The profile shows the frequent variations of paleoclimate, water level, paleosalinity, and redox conditions. Combining the variations of TOC content and paleoproductivity, the palaeoenvironmental evolution during the Es_3 period could divided into seven stages. These seven stages contains diverse features of OM enrichment, and are consistent with the divided stages in terms of the redox conditions.

Stage I ranged from the later Es_4 to early Es_3L (Fig. 14). During this stage, the climate was arid with low water levels and high salinity. The salinity was slightly hysteretic in response to climate change, which may be caused by the deposition and diagenesis process. The sediments in this stage were dominated by dark gray mudstones and salinastones. The thick salt layer in this stage may be caused by the dry climate which also led to the increasing salinity and stably stratified water column (Wu et al., 2016). The reduced condition at the bottom of the column facilitated OM preservation.

Stage II occurred in the middle of the Es_3L period. The climate was semi-humid at the beginning and transferred to arid at the end. The lithology was mainly gray mudstones and black shales with thin-bedded brown oil shales. During this stage, the water level was relatively high with reducing conditions, and the lake is eutrophic with relatively high paleoproductivity benefitting OM enrichment. A dry climate transitorily occurred at the end of this stage and formed the thin layer of white salt (Fig. 14). This thin salt provided good sealing conditions for the preservation of the previously enriched OM.

Stage III took place from the later Es_3L to early Es_3M, where the climate was relatively moist. The lithology was mainly dark gray mudstones. The moist climate caused relatively high water levels and decreasing salinity. The moist climate brought abundant terrigenous detritus and biological debris, which heightened the OM content (Fig. 14).

Stage IV was the early phases of the Es_3M period. The climate was relatively moist with relatively high water levels and low salinity. This stage was mainly dysoxic, which may be caused by oxygen invasion due to the tectonic activity (Figs. 1 and 2). The activity intensity of the Wending and Wendong fault systems was enhanced in this stage. The bottom of the lake was lifted, and formed the Wenliu uplift with two accompanying sags (Fig. 1c). This tectonism increased the accommodation space of the Es_3 Dongpu Lake Basin, which led to the input of a large number of foreign substances including aquatic plants, allochthonous OM, sand, and other detrital materials. The previous redox condition at the bottom of the lake was disrupted, and the paleoproductivity and TOC content in this stage were relatively low. A transiently arid climate occurred in the interval of stage IV, which may lead to rapid changes in the runoff and affect the water level, weathering and deposition, as well as salinity. The primary lithology at this stage consisted of dark gray mudstones and gray oil stain siltstones. The appeared siltstones at this stage were conduced to form sweet points for hydrocarbon accumulation, which made this segment favorable for shale oil exploration.

Stage V was from the later Es_3M to early Es_3U period. All palaeoenvironmental proxies changed dramatically at the beginning of this

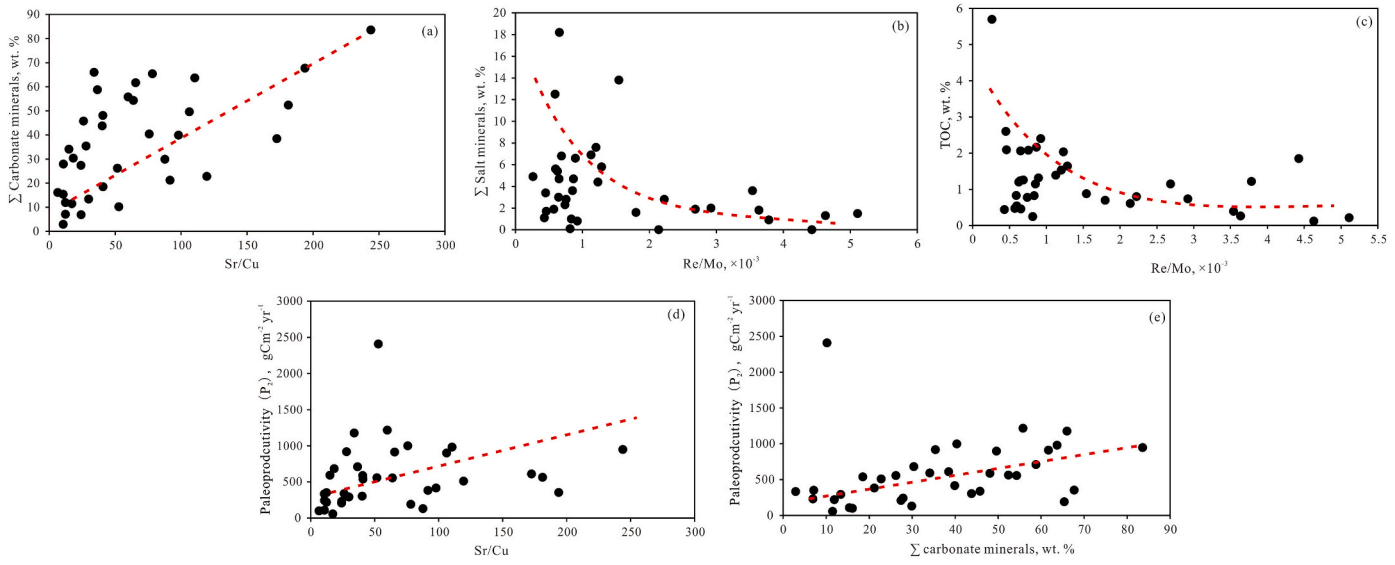

Fig. 13. Relationships between carbonate minerals and Sr/Cu (a); salt minerals and Re/Mo (b); TOC and Re/Mo (c); paleoproductivity and Sr/Cu (d); and paleoproductivity and carbonate minerals (e). Carbonate minerals are the sum of aragonite, calcite, ankerite, and dolomite. Salt is the sum of gypsum, anhydrite, and halite.

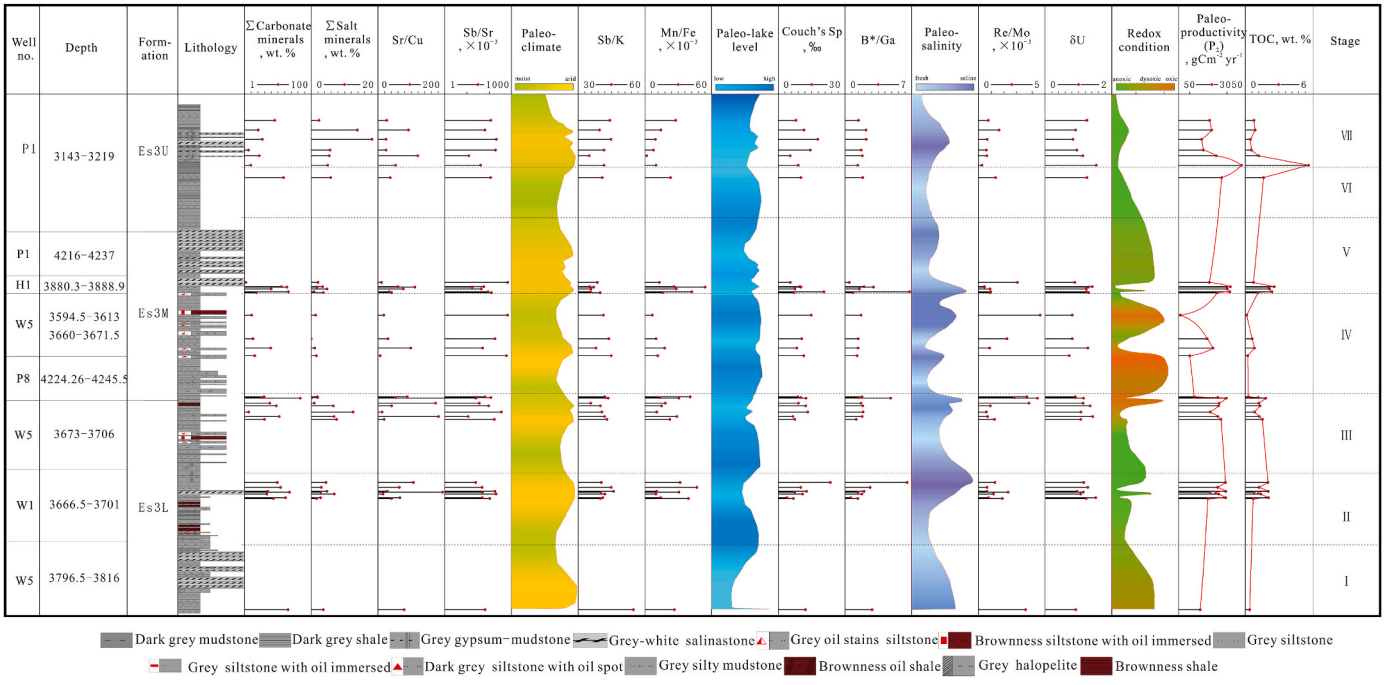

Fig. 14. Stratigraphic variation profile of multiple alternative palaeoenvironmental indicators for the Es_3 Formation in the Dongpu depression. ∑salt minerals is the sum of gypsum, anhydrite, and halite, and ∑carbonate minerals is the sum of aragonite, calcite, ankerite, and dolomite, and $\delta U = 2U/(U + Th/3)$.

stage. The lithology was dominated by white salinastones, followed by gray mudstones, implying that the climate was arid (Fig. 14). This arid climate led to low water levels and relatively high salinity. The paleo-productivity and TOC were relatively low, which may be caused by the relatively oxic conditions. Although the oxic conditions at this stage were not helpful for OM conservation, the thick salt provided an excellent seal-capping condition for the accumulation and preservation of OM generated at stages II, III, and IV.

Stage VI took place in the middle of the Es_3U period. The climate was humid, leading to high water levels and low salinity with reducing conditions. The lithology was mainly composed of dark gray shales and mudstones. In this stage, the Dongpu paleolake was eutrophic with high paleoproductivity, and abundant OM enriched in the sediments.

Stage VII took place in the latter part of the Es_3U period when the climate was arid and changed to humid later. Gray gypsum mudstones dominated the lithology with high carbonate minerals (Fig. 14). The arid climate led to low water levels and high salinity with the stratified water columns. The OM was well preserved under anoxic conditions at this stage, which facilitated the relatively high productivity and high TOC content. The thick gypsum and mudstones in this stage provided good cover for the preservation of OM generated in stage VI (Fig. 14).

6. Conclusions

In this study, mineralogical and geochemical methods were utilized to reconstruct the palaeoenvironment of Dongpu Ancient Lake Basin during the Es_3 period and analyze its effect on OM enrichment. The key conclusions are summarized as following: Es_3 shales primarily consist of gray mudstones and shales with interbedded white salinastones. Clay minerals dominate the Es_3 shales, followed by calcite and ankerite. Illite is predominant in clay minerals, followed by I/S, and no montmorillonite was observed. Gypsum, anhydrite, and halite have a non-negligible proportion. The salinastone is strongly associated with the palaeoenvironment. The paleoclimate during the Es_3 period had obvious influences on lake level, terrigenous input, paleoproductivity, as well as the redox conditions. Es_3 shales have abundant OM accumulation with high TOC content of 0.12–5.70 wt %. While, the OM distribution was affected by the salt content and shows obvious differences in different saline regions of Dongpu depression. During the Es_3 period of 445-38 Ma, the north SR of Dongpu depression has a drier climate, deeper water level, higher salinity, and more anoxic conditions than FR and BR. These palaeoenvironmental differences caused higher OM enrichments and higher salt content in the SR than those in FR and BR. In addition, the composite patterns of palaeoenvironmental variation affected the vertical anisotropy of OM enrichment. Furthermore, the palaeoenvironmental variation during the Es_3 period were classified seven stages, presenting obvious anisotropy of OM enrichment. Stages I, V, and VII deposited thick salt under an arid climate, and provided an excellent seal-capping and preservation condition for OM enriched at stages II, III, IV, and VI. The shale reservoirs deposited in stages III and IV were favorable for shale oil exploration.

Credit author statement

Fujie Jiang, Doctor, professor; the supervisor and funder of this study, provided the systematic guidance for this study and manuscript, Di Chen, Doctor, designed and execute this study work from beginning to end, and drafted and revised this manuscript. Kangchao Ning, the expert of China Coal Jiangnan Construction and Development Group Co., provide huge help for the sampling and experiment. Chenxi Zhu, providing the help for modify this manuscript and the revision. Lin Ma, Doctor, The University of Manchester, Henry Moseley X-ray Imaging Facility; method guidance and language instructor. Tianwu Xu, Doctor, the expert of Research Institute of Exploration and Development, SINOPEC Zhongyuan Oilfield Company, provided the help of well sampling and the geological guidance, and reviewed this manuscript. Ru Qin, provided the help of well sampling and experiment. Boshi Li, providing the help for the help of disposal data, literature research and manuscript. Yuanyuan Chen, provide help for data processing. Lina Huo, Master, providing the help of manuscript editing and drawing. Zhi Xu, Master, providing the help of manuscript editing.

Declaration of competing interest

The authors declare that they have no known competing financial interests or personal relationships that could have appeared to influence the work reported in this paper.

Acknowledgments

This research was funded by the National Natural Science Foundation of China (NSFC) (41872118), the Science Foundation of China University of Petroleum, Beijing (No. 2462020YXZZ021), the Youth Program of National Natural Science Foundation of China (Grant No. 41802148). We are grateful to Sinopec Zhongyuan Oilfield for their support and help in this study. We appreciate to Dr. Wenyao Xiao at Nanjing University for his laboratory assistance and suggestion. We express our heartfelt thanks to Dr. Wei Li at the University of Nottingham for their great efforts in refining the English of the manuscript.

References

Bao, L.N., 2009. Cretaeous Dinoflagellates, Chlorophytes and Acritarchs, and its Genetic Potential from the Songliao Basin. China University of Geosciences.
Cai, X., 2012. Hydrocarbon generation-expulsion mechanisms and efficiencies of lacustrine source rocks: a case study from the Dongying sag, Bohai Bay basin. Oil Gas Geol. 33, 329–334 (in Chinese with English Abstract).
Chen, J., Lu, K., Feng, Y., Yuan, K., Wang, D., Cui, H., Zhang, W., 2012. Evaluation on hydrocarbon source rocks in different environments and characteristics of hydrocarbon generation and expulsion in Dongpu Depression. Fault-Block Oil Gas Field 19 (1), 35–38.
Chen, S., Xu, S., Wang, D., Tan, Y., 2013. Effect of block rotation on fault sealing: an example in Dongpu sag, Bohai Bay basin, China. Mar. Petrol. Geol. 39 (1), 39–47.
Chivas, A.R., Deckker, P., Shelley, J.M.G., 1986. Strontium content of ostracods indicates paleosalinity. Nature 316, 251–253.
Couch, E.L., 1971. Calculation of paleosalinities from boron and clay mineral data. AAPG Bull. 55 (10), 1829–1837.
Crusius, J., Calvert, S., Pedersen, T., Sage, D., 1996. Rhenium and molybdenum enrichments in sediments as indicators of oxic, suboxic and sulfidic conditions of deposition. Earth Planet Sci. Lett. 145, 65–78.
Curtis, C., 1964. Studies on the use of boron as a paleoenvironmental indicator. Geochem. Cosmochim. Acta 28 (7), 1125–1137.
Dean, W.E., Gardner, J.V., Piper, D.Z., 1997. Inorganic geochemical indicators of glacial-interglacial changes in productivity and anoxia on the California continental margin. Geochem. Cosmochim. Acta 61 (21), 4507–4518.
Deckker, P., Chivas, A.R., Shelley, J.M.G., Torgersen, T., 1988. Ostracod shell chemistry: a new palaeoenvironmental indicator applied to a regressive transgressive record from the Gulf of Carpentaria. Palaeogeogr. Palaeoclimatol. Palaeoecol. 66, 231–241.
Drexler, J.Z., Paces, J.B., Alpers, C.N., Windham-Myers, L., Neymark, L.A., Bullen, T.D., Taylor, H.E., 2014. $^{234}U/^{238}U$ and $\delta^{87}Sr$ in peat as tracers of paleosalinity in the Sacramento-San Joaquin Delta of California, USA. Appl. Geochem. 40, 164–179.
Du, H., Yu, X., Chen, F., 2008. Sedimentary characteristics of saltrocks and their petroleum geologic significance of the member 3 of Shahejie formation of Paleogene in Dongpu depression, Henan Province. J. Palaeogeogr. 10, 53–62.
Dutta, S., Mathews, R.P., Singh, B.D., Tripathi, S.M., Singh, A., Saraswati, P.K., Banerjee, S., Mann, U., 2011. Petrology, palynology and organic geochemistry of Eocene lignite of Matanomadh, Kutch Basin, western India: implications to depositional environment and hydrocarbon source potential. Int. J. Coal Geol. 85 (1), 91–102.
Farhaduzzaman, M., Abdullah, W., Islam, M., 2012. Depositional environment and hydrocarbon source potential of the permian gondwana coals from the barapukuria basin, northwest Bangladesh. Int. J. Coal Geol. 90, 162–179.
Fu, C.Y., 2015. Exploration and Development of Unconventional Petroleum resources [M]. China Petrochemical Press, Beijing.
Grosjean, E., Love, G.D., Stalvies, C., Fike, D.A., Summons, R.E., 2009. Origin of petroleum in the neoproterozoice cambrian south Oman salt basin. Org. Geochem. 40, 87–110.
Hao, F., Zhou, X., Zhu, Y., Yang, Y., 2011. Lacustrine source rock deposition in response to co-evolution of environments and organisms controlled by tectonic subsidence and climate, Bohai Bay Basin. China. Org. Geochem. 42, 323–339.
Henderson, G.M., 2002. New oceanic proxies for paleoclimate. Earth Planet Sci. Lett. 203 (1), 1–13.
Hou, G., Qian, X., Cai, D., 2001. The tectonic evolution of Bohai basin in Mesozoic and Cenozoic time. Acta Sci. Nat. Univ. Pekin. 37, 845–851 (in Chinese).
Huang, R., Zhu, C., Wang, S., 2007. Magnetic susceptibility and Rb/Sr ratio of peat stratum in Tiantangzhai and its significance of palaeoclimate. Sci. Geogr. Sin. 27 (3), 385–389 (in Chinese).
Ishiwatari, R., Yamamoto, S., Uemura, H., 2005. Lipid and lignin/cutin compounds in Lake Baikal sediments over the last 37 kyr: implications for glacial-interglacial palaeoenvironmental change. Org. Geochem. 36, 327–347.
Ishiwatari, R., Negishi, K., Yoshikawa, H., Yamamoto, S., 2009. Glacial-inter-glacial productivity and environmental changes in Lake Biwa, Japan: a sediment core study of organic carbon, chlorins andbiomarkers. Org. Geochem. 40 (4), 520–530.
Jiang, F., Chen, D., Wang, Z., Xu, Z., Liu, Y., 2016a. Pore characteristic analysis of a lacustrine shale: a case study in the Ordos Basin, NW China. Mar. Petrol. Geol. 73, 554–571.
Jiang, F., Chen, D., Chen, J., Li, Q., Liu, Y., Shao, X., Hu, T., Dai, J., 2016b. Fractal analysis of shale pore structure of continental gas shale reservoir in the Ordos Basin, NW China. Energy Fuel. 30 (6), 4676–4689.
Jiang, S., Chen, Y., Ling, H., Yang, J., Feng, H., Ni, P., 2006. Trace-and rare-earth element geochemistry and Pb-Pb dating of black shales and intercalated Ni-Mo-PGE-Au sulfide ores in Lower Cambrian strata, Yangtze Platform, South China. Miner. Deposita 41 (5), 453–467.
Jiang, Y., Chang, Z., Lu, X., Wu, X., 2008. Genetic types and distribution of paleogene condensate gas pools in Dongpu depression. J. China Univ. Petrol. 32 (5), 28–34 (Edition of Natural Science).
Jin, Q., Zhu, G., Wang, J., 2008. Deposition and distribution of high- potential source rocks in saline lacustrine environments. J. Chin. Univ. Petrol. 32, 19–23 (in Chinese with English Abstract).
Jones, B., Manning, D., 1994. Comparison of geochemical indices used for the interpretation of palaeoredox conditions in ancient mudstones. Chem. Geol. 111 (1–4), 111–129.
Katz, B., Lin, F., 2014. Lacustrine basin unconventional resource plays: key differences. Mar. Petrol. Geol. 56, 255–265.
Klinkhammer, G., Palmer, M., 1991. Uranium in the oceans: where it goes and why. Geochem. Cosmochim. Acta 55 (7), 1799–1806.
Learman, A., 1989. Lakes Chemistry Geology Physics. Translation. In: Wang, S., et al. (Eds.). Geology Press, Bejing, pp. 316–318.
Li, C., Kang, S., Zhang, Q., Wang, F., 2009. Rare earth elements in the surface sediments of the yarlung tsangbo (upper brahmaputra river) sediments, southern Tibetan plateau. Quat. Int. 208, 151–157.
Li, G.S., Wang, Y.B., Lu, Z.S., Liao, W., Song, G.Q., Wang, X.J., Xu, X.Y., 2014. Geobiological processes of the formation of lacustrine source rock in Paleogene. Sci. Sin. (6), 1206–1217, 000.
Li, S., Zheng, D., Geng, F., 2002. An attempt on quantitative calculation of lake palaeoproductivity. Geol. J. China Univ. 8 (2), 215–219.
Li, W., Zhang, Z., Li, Y., Liu, C., Fu, N., 2013. The main controlling factors and developmental models of Oligocene source rocks in the Qiongdongnan Basin, northern South China Sea. Petrol. Sci. 10 (2), 161–170.
Li, W., Lu, S., Xue, H., Zhang, P., Hu, Y., 2015a. Oil content in argillaceous dolomite from the Jianghan Basin, China: application of new grading evaluation criteria to study shale oil potential. Fuel 143, 424–429.
Li, W., Lu, S., Xue, H., Zhang, P., Wu, S., 2015b. The formation environment and developmental models of argillaceous dolomite in the Xingouzui Formation, the Jianghan Basin. Mar. Petrol. Geol. 67, 692–700.
Lipinski, M., Warning, B., Brumsack, H., 2003. Trace metal signatures of jurassic/cretaceous black shales from the Norwegian shelf and the barents Sea. Palaeogeogr. Palaeoclimatol. Palaeoecol. 190, 459–475.
Liu, C., Xu, J., 2002. Estimation method on productivity of oil-producing lake and a case study. Acta Sedimentol. Sin. 20 (1), 144–149.
Liu, C., Liu, K., Wang, X., Wu, L., Fan, Y., 2018. Chemostratigraphy and sedimentary facies analysis of the permian lucaogou Formation in the jimusaer sag, junggar basin, NW China: implications for tight oil exploration. J. Asian Earth Sci. org/10.1016/j.jseaes.2018.04.013.
Liu, G., Zhou, D., 2007. Application of microelements analysis in identifying sedimentary environment. Petrol. Geol. Exp. 29 (3), 307–314.
Liu, J.D., Jiang, Y.L., Tan, Y.M., Mu, X.S., 2014. Relationship between oil and gas in Dongpu sag, Bohai Bay Basin. Acta Sedimentol. Sin. 32 (1), 126–137 (in Chinese).
Lu, R., Zhao, C., Chen, S., 1993. Petroleum Geology of China, vol. 7. Petroleum Industry Press, Beijing. Zhongyuan Oilfield.
Lyu, X., Jiang, Y., Liu, J., 2016. Phase types identification and genetic analysis for Paleogene condensate gas pools in the Dongpu depression. J. China Univ. Min. Technol. 45 (6), 1148–1155.
Mayer, B., Schwark, L., 1999. A 15,000-year stable isotope record from sediments of Lake Steisslingen, Southwest Germany. Chem. Geol. 161 (1), 315–337.
McLennan, S.M., Hemming, S., Taylor, S.R., Eriksson, K.A., 1995. Early Proterozoic crustal evolution: geochemical and Nd-Pb isotopic evidence from metasedimentary rocks, southwestern North America. Geochem. Cosmochim. Acta 59, 1153–1177.
Morel, F.M.M., Price, N.M., 2003. The biogeochemical cycles of trace metals in the oceans. Science 300 (5621), 944–947.
Müller, P.J., Suess, E., 1979. Productivity sedimentation rate, andsedimentary organic matter in the oceans: 1.Organic carbonpreservation. Deep-Sea Res. 26 (12), 1347–1362.
Ning, K., 2017. Comparison of Characteristics of Source Rocks of Salt Zone and Saltless Zone, Dongpu Depression- as an Example from Third Member of Shahejie Formation. China University of Petroleum (Beijing), master's thesis.
Paytan, A., Griffith, E.M., 2007. Marine barite: recorder of variations in ocean export productivity. Deep-Sea Re-search II. https://doi.org/10.1016/j.dsr2.2007.01.007.
Pecharsky, V.K., Zavalij, P.Y., 2003. Fundamentals of Powder Diffraction and Structural Characterization of Minerals. Kluwer Academic Publishers, New York, p. 713.
Pedersen, T.F., Calvert, S.E., 1990. Anoxia vs. Productivity: what controls the formation of organic-carbon-rich sediments and sedimentary rocks? AAPG Bull. 74 (4), 545-466.
Peters, K.E., Cunningham, A.E., Walters, C.C., Jiang, J., Fan, Z., 1996. Petroleum systems in the jiangling - dangyang area, Jianghan Basin. China. Org. Geochem. 24, 1035–1060.

Petersen, H.I., Nytoft, H.P., 2006. Oil generation capacity of coals as a function of coal age and aliphatic structure. Org. Geochem. 37 (5), 558–583.
Philp, R.P., Fan, Z., 1987. Geochemical investigation of oils and source rocks from qianjiang depression of Jianghan basin, aterrigenous saline basin, China. Org. Geochem. 11 (6), 549–562.
Piper, D., 1994. Seawater as the source of minor elements in black shales, phosphorites and other sedimentary rocks. Chem. Geol. 114 (1–2), 95–114.
Qi, J., Yang, Q., 2010. Cenozoic structural deformation and dynamic processes of the Bohai Bay Basin province, China. Mar. Petrol. Geol. 27 (4), 757–771.
Roy, D.K., Roser, B.P., 2013. Climatic control on the composition of carboniferouspermian gondwana sediments, Khalaspir basin. Bangladesh. Gondwana Res. 23 (3), 1163–1171.
Scheffler, K., Hoernes, S., Schwark, L., 2003. Global changes during Carboniferous-Permian glaciation of Gondwana: linking polar and equatorial climate evolution by geochemical proxies. Geology 31, 605–608.
Schieber, J., Zimmerle, W., 1998. The history and promise of shale research. Shales and Mudstones 1, 1–10.
Schröder, S., Grotzinger, J.P., 2007. Evidence for anoxia at the Ediacaran-Cambrian boundary: the record of redox-sensitive trace elements and rare earth elements in Oman. J. Geol. Soc. 164 (1), 175–187.
Shao, L., Stettegger, K., Garbe-Schoenberg, C.D., 2001. Sandstone petrology and geochemistry of the Turpan basin (NW China): implications for the tectonic evolution of a continental basin. J. Sediment. Res. 71, 37–49.
Song, M., 2005. Sedimentary environment geochemistry in the Sha-4 section of southern ramp, dongying depression. J. Mineral. Petrol. 25 (1), 67–73, 03.
Sonnenberg, S.A., Pramudito, A., 2009. Petroleum Geology of the giant elm coulee field, Williston Basin. AAPG Bull. 93, 1127–1153.
Steiner, M., Wallis, E., Erdtmann, B., Zhao, Y., 2001. Submarine-hydrothermal exhalative ore layers in black shales from South China and associated fossils-insights into a Lower Cambrian facies and bio-evolution. Palaeogeogr. Palaeoclimatol. Palaeoecol. 169 (3–4), 165–191.
Stow, D.A.V., Huc, A.Y., Bertrand, P., 2001. Depositional processes of black shales in deep water. Mar. Petrol. Geol. 18, 491–498.
Su, H., Qu, L., Zhang, J., Wang, P., He, F., Wang, M., Wang, Q., Hu, Y., 2006. Tectonic evolution and extensional pattern of rifted basin, a case study of Dongpu depression. Oil Gas Geol. 27 (1), 70–71 (in Chinese with English abstract).
Sun, J.L., Schechter, D., Huang, C.K., 2016. Grid-sensitivity analysis and comparison between unstructured perpendicular bisector and structured tartan/local-grid refinement grids for hydraulically fractured horizontal wells in Eagle Ford Formation with complicated natural fractures. SPE J. https://doi.org/10.2118/177480-PA.
Sun, Q., Jia, Y., Shen, H., Zhang, J., Yu, L., 2010. Distribution and environmental implication of Rb, Sr in the holocene lacustrine sediments of huangqihai lake, inner Mongolia. J. Palaeogeogr. 12 (4), 444–450.
Taylor, S.R., McLennan, S.M., 1985. The Continental Crust: its Composition and Evolution. Blackwell, Oxford, p. 312.
Walker, C.T., Price, N.B., 1963. Departure curves for computing paleosalinity from boron in illites and shales. AAPG Bull. 47 (5), 833–841.
Wang, M., Huang, C., Xu, Z., Chen, J., Yang, S., 2006. Review on paleosalinity recovery in sedimentary environment. Xinjiang Oil Gas 2 (1), 9–12.
Wang, M., Sherwood, N., Li, Z., Lu, S., Wang, W., Huang, A., Peng, J., Luc, K., 2015. Shale oil occurring between salt intervals in the Dongpu depression, Bohai Bay Basin, China. Int. J. Coal Geol. 152, 100–112.
Wang, Q.F., Jiang, F.J., Ji, H.C., Jiang, S., Guo, F.X., Gong, S.Y., Wang, Z., Liu, X.H., Li, B. S., Chen, Y.Y., Deng, Q., 2020. Differential enrichment of organic matter in saline lacustrine source rocks in a rift basin: a case study of Paleogene source rocks, Dongpu Depression, Bohai Bay Basin. Nat. Resour. Res. 29 (6), 4053–4072.
Wang, S., Huang, X., Tuo, J., Shao, H., Yan, C., Wang, S., He, Z., 1997. Evolutional characteristics and their paleoclimate significance of trace elements in the HeTaoYuan formation, Biyang depression. Acta Sedimentol. Sin. (1), 66–71.
Wignall, P.B., Myers, K.J., 1988. Interpreting benthic oxygen levels in mudrocks: a new approach. Geology 16, 452–455.
Wu, C., Yang, C., Chen, Q., 1999. The origin and geochemical characteristics of upper sinain_lower cambrian black shales in Western Hunan. Acta Petrol. Mineral. (1), 28–29.
Wu, H., Hu, W., Cao, J., Wang, X., Wang, X., Liao, Z., 2016. A unique lacustrine mixed dolomitic-clastic sequence for tight oil reservoir within the middle Permian Lucaogou Formation of the Junggar Basin, NW China: reservoir characteristics and origin. Mar. Petrol. Geol. 76, 115–132.
Wu, L., Wang, F., Wang, D., Fu, M., Jia, Y., 2018. The lithologic differences between the third and fourth members of the Eocene Shahejie Formation in the Bohai Bay Basin and the associated climatic evolution. Geol. J. 53 (3), 788–802.
Xiong, X., Xiao, J., 2011. A summary of geochemical indicators of sedimentary environments. Earth Environ. 39 (3), 405–414.
Yan, D., Wang, H., Fu, Q., Chen, Z., He, J., Gao, Z., 2015. Geochemical characteristics in the longmaxi formation (early silurian) of south China: implications for organic matter accumulation. Mar. Petrol. Geol. 65, 290–301.
Yan, L.J., Zheng, M.P., 2015. The response of lake variations to climate change in the past forty years: a case study of the northeastern Tibetan Plateau and adjacent areas, China. Qut. Int. 371, 31–48.
Yang, Y., Fang, X., Appel, E., Galy, A., Li, M., Zhang, W., 2013. Late Pliocene-Quaternary evolution of redox conditions in the western Qaidampaleolake (NE Tibetan Plateau) deducedfrom Mn geochemistry in the drilling core SG-1. Quat. Res. 80, 586–595.
Ye, C., Yang, Y., Fang, X., Zhang, W., 2016. Late Eocene clay boron-derived paleosalinity in the Qaidam Basin and its implications for regional tectonics and climate. Sediment. Geol. 346, 49–59.
Zhang, W., Yang, H., Fu, S., Zan, C., 2007. On the development mechanism of the lacustrine high-grade hydrocarbon source of Chang 91 member in Ordos Basin. Sci. China Earth Sci. 50, 39–46.
Zhang, P, Zhang, J C, Huang, Y Q, 2015. The lithofacies characteristics of Es3 in the Northern Dongpu Depression. Sci. Technol. Eng 2015, 21.
Zhu, C., Jiang, F., Zhang, P., Hu, T., Liu, Y., Xu, T., Zhang, Y., Deng, Q., Zhou, Y., Xiong, H., Song, Z., 2021. Identification of effective source rocks in different sedimentary environments and evaluation of hydrocarbon resources potential: a case study of paleogene source rocks in the Dongpu Depression, Bohai Bay Basin. J. Petrol. Sci. Eng. 108477.